FINAL REPORT
April 1, 1997 – December 31, 2000
Grant No. F49620-97-1-0234

PROCESSING AND PROPERTIES OF Al-Li-Cu-X ALLOYS

Submitted to:

Dr. Craig S. Hartley, Program Manager
Metallic Materials Program
Directorate of Aerospace and Mechanical Sciences
Air Force Office of Scientific Research
801 N. Randolph Street
Arlington, VA 22203-1977

Submitted by:

Edgar A. Starke, Jr.
Earnest Oglesby Professor

SEAS Report No. UVA/525869/MSE01/101

DEPARTMENT OF MATERIALS SCIENCE AND ENGINEERING

SCHOOL OF
ENGINEERING
& APPLIED SCIENCE

University of Virginia
Thornton Hall
Charlottesville, VA 22903

UNIVERSITY OF VIRGINIA
School of Engineering and Applied Science

The University of Virginia's School of Engineering and Applied Science has an undergraduate enrollment of approximately 1,500 students with a graduate enrollment of approximately 600. There are 160 faculty members, a majority of whom conduct research in addition to teaching.

Research is a vital part of the educational program and interests parallel academic specialties. These range from the classical engineering disciplines of Chemical, Civil, Electrical, and Mechanical and Aerospace to newer, more specialized fields of Applied Mechanics, Biomedical Engineering, Systems Engineering, Materials Science, Nuclear Engineering and Engineering Physics, Applied Mathematics and Computer Science. Within these disciplines there are well equipped laboratories for conducting highly specialized research. All departments offer the doctorate; Biomedical and Materials Science grant only graduate degrees. In addition, courses in the humanities are offered within the School.

The University of Virginia (which includes approximately 2,000 faculty and a total of full-time student enrollment of about 17,000), also offers professional degrees under the schools of Architecture, Law, Medicine, Nursing, Commerce, Business Administration, and Education. In addition, the College of Arts and Sciences houses departments of Mathematics, Phyics, Chemistry and others relevant to the engineering research program. The School of Engineering and Applied Science is an integral part of this University community which provides opportunities for interdisciplinary work in pursuit of the basic goals of education, research, and public service.

REPORT DOCUMENTATION PAGE

AFRL-SR-BL-TR-01-

0144

1. REPORT DATE (DD-MM-YYYY)	2. REPORT TYPE	3. DATES COVERED (From - To)
2 Feb 2001	Final	4/1/97 – 12/31/00

4. TITLE AND SUBTITLE
Processing and Properties of Al-Li-Cu-X Alloys

5a. CONTRACT NUMBER

5b. GRANT NUMBER
AFOSR Grant No. F49620-97-1-0234

5c. PROGRAM ELEMENT NUMBER

6. AUTHOR(S)
Edgar A. Starke, Jr.

5d. PROJECT NUMBER

5e. TASK NUMBER

5f. WORK UNIT NUMBER

7. PERFORMING ORGANIZATION NAME(S) AND ADDRESS(ES)
Department of Materials Science and Engineering
University of Virginia
116 Engineer's Way, P.O. Box 400745
Charlottesville, VA 22904-4745

8. PERFORMING ORGANIZATION REPORT NUMBER

9. SPONSORING/MONITORING AGENCY NAME(S) AND ADDRESS(ES)
Air Force Office of Scientific Research
801 North Randolf Street
Room 732
Arlington, VA 22203-1977

10. SPONSOR/MONITOR'S ACRONYM(S)

11. SPONSOR/MONITOR'S REPORT NUMBER(S)

12. DISTRIBUTION/AVAILABILITY STATEMENT

13. SUPPLEMENTARY NOTES

14. ABSTRACT
The objectives of this research were to identify the mechanisms for the large difference in ductility between the near peak aged AF/C-489 and AF/C 458 and then develop an aging schedule to optimize the microstructure for high strength and ductility. Duplex aging treatments produced significant increases in ductility for AF/C-489, approaching that of AF/C-458. Although strain localization occurred in both alloys it was more severe in AF/C-489 due to the higher volume fraction of shearable delta prime and a much larger grain size. Our results show that a significant increase in ductility of the higher lithium AF/C-489 can be obtained by double aging and reducing the grain size. The report describes the details of the study and the optimum processing to obtain this goal.

15. SUBJECT TERMS

16. SECURITY CLASSIFICATION OF:			17. LIMITATION OF ABSTRACT	18. NUMBER OF PAGES	19a. NAME OF RESPONSIBLE PERSON
a. REPORT	b. ABSTRACT	c. THIS PAGE			19b. TELEPHONE NUMBER (Include area code)

Final Report

PROCESSING & PROPERTIES OF AL-LI-CU-X ALLOYS
AFOSR Grant No. F49620-97-1-0234

Dr. Edgar A. Starke, Jr.
Department of Materials Science and Engineering
University of Virginia
116 Engineer's Way
P.O. Box 400745
Charlottesville, VA 22904-4745

INTRODUCTION

The optimization of thermomechanical processing is a paramount consideration for Al-Li-Cu-X alloys. The microstructural evolution, and therefore the mechanical properties, of these alloys may be dramatically altered through precise changes in various processing stages. Primarily, the imposed cooling rate from the solution heat treatment temperature and the amount of introduced plastic deformation prior to aging have marked effects on both the competitive microstructural evolution and subsequent mechanical properties. Other important metallurgical factors, such as texture and grain size, have been shown to dictate the ductility of this class of alloys. It is necessary to understand each of these thermomechanical-processing steps to truly optimize the performance of this alloy system.

Although Al-Li-Cu alloys showed initial promise as lightweight structural materials, implementation into primary aerospace applications has been hindered due in part to their characteristic anisotropic mechanical and fracture behaviors. The Air Force recently developed two isotropic Al-Li-Cu-X alloys with 2.1 wt pct Li and 1.8 wt pct Li designated AF/C-489 and AF/C-458, respectively. The elongation at peak strength was less than the required 5 pct for the 2.1 wt pct Li variant but greater than 10 pct for the 1.8 wt pct Li alloy. The objectives of our investigations were to first identify the mechanisms for the large difference in ductility between the AF/C-489 and AF/C-458 alloys and then to develop an aging schedule to optimize the microstructure for high ductility and strength levels.

MATERIALS

Our study focused on the two Air Force alloys;

AF/C-458: Al - 2.7 Cu – 1.8 Li – 0.6 Zn – 0.3 Mg – 0.3 Mn – 0.08 Zr
AF/C-489 : Al – 2.7 Cu – 2.1 Li – 0.6 Zn – 0.3 Mg – 0.3 Mn – 0.05 Zr

The AF/C-458 alloy was fabricated at Alcoa commercial facilities, while AF/C-489 was a laboratory alloy from Wright Patterson Air Force Base. These alloys were received as plate of 3/4" and 0.5" thick, respectively. Both alloys were received in the unrecrystallized condition consisting of 5-10μm sub-grains. However, the grain size for the AF/C-489 was considerably larger than the grain size for the AF/C-458.

EFFECT OF PRECIPITATE AND GRAIN STRUCTURE ON DUCTILITY

The precipitation response for both the AF/C-489 and AF/C-458 alloys was determine by TEM and DSC, and used to design an improved microstructure through duplex aging for AF/C-489. Duplex aging of the AF/C-489 alloy resulted in significant increases in ductility by as much as 85% with a small decrease of only 6.5% and 2.5% in yield and ultimate tensile strength, respectively. No significant improvements were found with either of the duplex or triple aging practices for the AF/C-458 commercial alloy indicating a large processing window. Quantitative TEM demonstrated that the precipitation response significantly differed between the duplex aging for the AF/C-489 and AF/C-458 alloys. The duplex aged AF/C-489 alloy competitively precipitated more θ" at the expense of T_1 whereas no significant changes in precipitation response occurred for the AF/C-458 alloy. Furthermore, shearable δ' volume fraction was calculated to be on average ~3.0% greater in the AF/C-489 than the AF/C-458 alloy. Conventional TEM also demonstrated that grain boundary T_1 precipitation was unaffected by duplex aging designed to competitively precipitate more matrix T_1 than grain boundary T_1. In fact, all investigated single and double aged samples contained grain boundary T_1.

Conventional TEM, HREM, and SEM fractography demonstrated that formation of shear bands occurred as a result of the localized shearing of both the δ' and T_1 strengthening precipitates in both the AF/C-458 and AF/C-489 alloys. Our results indicated that the low ductility of the AF/C-489 alloy in comparison to the AF/C-458 alloy is attributed to the increased volume fraction of shearable δ' coupled with a larger grain size, both of which significantly increase the amount of strain localization and stress concentrations at grain boundaries. This results in more low energy intergranular fracture for the AF/C-489 alloy. The details of this phase of our research can be found in the publication: "The Effect of Processing and Microstructure Development on the Slip and Fracture Behavior of the 2.1 Wt Pct Li AF/C-489 and 1.8 Wt Pct Li AF/C-458 Al-Li-Cu-X Alloys," A.A. Csontos and E.A. Starke, Jr., Metallurgical and Materials Transactions A., Vol. 31A, August 2000, pp. 1965-1976, attached as Appendix I.

THE EFFECT OF PLASTIC DEFORMATION ON COMPETITIVE PRECIPITATION

The role of plastic deformation prior to artificial aging on the microstructural evolution and mechanical properties of the AF/C 458 was investigated. Induced plastic deformation ranged from a non-stretched or 0% stretch condition to an 8% stretch, with intermediate stretches of 2%, 4% and 6%. Tensile properties, fractography and quantitative precipitate analysis were acquired from specimens that were water quenched from a solution heat treatment, immediately stretched and artificially aged at 150°C. Fractography was investigated through scanning electron microscopy (SEM). Quantitative transmission electron microscopy (TEM) determined the variation in precipitate type, number density, size and volume fraction of the major strengthening precipitates Al_2CuLi (T_1), Al_2Cu (θ'/θ') and Al_3Li (δ). Age hardening curves for each level of mechanical stretch illustrated the enhanced aging kinetics of plastically deformed material. Quantitative TEM indicated that increasing amounts of pre-age stretch were found to greatly affect the competitive precipitation kinetics of T_1 and θ"/θ' in AF/C 458 augmenting the volume fraction of fine matrix T_1 plates and dramatically decreasing the volume fraction of θ"/θ' for isochronal treatments. A quantitative microstructural comparison of specimens exhibiting a given strength demonstrated that the imposed level of cold work dictated the density, size and

volume fraction of the competing precipitates. The tensile data indicated a trend of increasing ductility for equivalent yield strengths with the increasing amount of pre-age mechanical stretch and therefore shorter artificial aging times. The quantitative precipitate data was used with a computer simulation for yield strength determination. The theoretical simulation reported calculated yield strengths in good accord with experimental results and can thus be used to predict the optimum microstructural configuration for high strength. The details of this phase of our research can be found in the publication: "The Role of Plastic Deformation on the Competitive Microstructural Evolution and Mechanical Properties of a Novel Al-Li-Cu-X Alloy," B.M. Gable, A.W. Zhu, A.A. Csontos and E.A. Starke, Jr., Journal of Light Metals, Vol. 1, No. 1, January 2001, pp. 1-14, attached as Appendix II.

EFFECT OF QUENCH RATE ON MICROSTRUCTURE AND PROPERTIES

The objective of this phase of our research was to determine the effect of quench rate on the microstructure and mechanical properties of the AF/C-458 and AF/C-489 alloys. TEM, SEM, microhardness and tensile testing were utilized to ascertain these microstructure/property relationships for both alloys in the T4, T6 and T86 tempers as a function of quench rate. Subsequent losses in ductility for both alloys in all tempers with decreasing quench rate were determined to be due to the precipitation of the equilibrium Al_2CuLi (T_1) phase along subgrain and grain boundaries which promoted intergranular fracture. Furthermore, yield and tensile strengths increased for both alloys in the T4 temper but decreased in the T6 and T86 tempers with decreasing quench rate. The increased strengths for the T4 condition resulted from the heterogeneous precipitation of coarse T_1 and naturally aged δ' phases. The decrease in yield and tensile strength for the T6 and T86 tempers were also due to the coarse heterogeneous precipitation of T_1 which denuded regions of Cu thereby reducing the number density of fine matrix θ'' (T6) and T_1 (86). Finally, a comparison of the quench sensitivity for both the AF/C-458 and AF/C-489 alloys indicates that the mechanical properties for both alloys were less quench rate sensitive than other typical Al-Li-Cu-X alloys. The details of this phase of our research can be found in the publication: "The Effect of Quench Rate on the Microstructure and Properties of AF/C-458 and AF/C-489 Al-Li-Cu-X Alloys," A.A. Csontos, B.M. Gable, A. Gaber and E.A. Starke, Jr., Materials Science Forum, Vols. 331-337, July 2000, pp. 1333-1340, attach as Appendix III.

PERSONAL SUPPORTED

Aladar A. Csontos	Graduate Student, University of Virginia
Brian M. Gable	Graduate Student, University of Virginia
Dr. Aiwu Zhu	Postdoctoral Scientist, University of Virginia
Dr. Edgar A. Starke, Jr.	University and Ogelsby Professor, University of Virginia

DEGREES GRANTED

Brian M. Gable, "The Role of Mechanical Stretch on the Microstructural Evolution of AF/C-458," Master of Science Degree, University of Virginia, May, 2000.

Aladar A. Csontos, "Microstructural Effects on the Slip & Fracture Behavior of Isotropic Al-Li-Cu-X Alloys," Doctor of Philosophy Degree in Materials Science and Engineering, University of Virginia, February 2001.

PUBLICATIONS

"Computer Experiment on Superposition of Strengthening Effects of Different Particles," A.W. Zhu, A. Csontos and E.A. Starke, Jr., **Acta Materialia, vol. 47,** June 1999, pp. 1713-1721.

"Need for New Materials in Aging Aircraft Structures," R.J. Bucci, C.J. Warren and E.A. Starke, Jr., **Journal of Aircraft, vol. 37,** January-Feburary 2000, pp. 122-129.

"The Effect of Quench Rate on the Microstructure and Properties of AF/C 458 and AF/C 489 Alloys", A.A. Csontos, B.M. Gable, A.F. Gaber and E.A. Starke, Jr., **Materials Science Forum, vol. 331-337**, April 2000, pp. 1333-1340.

"The Role of Mechanical Stretch on the Processing-Microstructure-Property Relationships of AF/C 458", B.M. Gable, A.A. Csontos and E.A. Starke, Jr., **Materials Science Forum, vol. 331-337,** April 2000, pp. 1341-1346.

"The Effect of Processing and Microstructure Development on the Slip and Fracture Behavior of the 2.1wt pct Li AF/C 489 and 1.8wt pct Li AF/C 458 Al-Li-Cu-X Alloys", A.A. Csontos and E.A. Starke, Jr., **Metallurgical and Materials Transactions A, vol. 31A**, August 2000, pp. 1965-1976.

"The Role of Plastic Deformation on the Competitive Microstructural Evolution and Mechanical Properties of a Novel Al-Li-Cu-X Alloy," **Journal of Light Metals, vol. 1,** January 2001, pp. 1-14.

The Effect of Processing and Microstructure Development on the Slip and Fracture Behavior of the 2.1 Wt Pct Li AF/C-489 and 1.8 Wt Pct Li AF/C-458 Al-Li-Cu-X Alloys

A.A. CSONTOS and E.A. STARKE, Jr.

Although Al-Li-Cu alloys showed initial promise as lightweight structural materials, implementation into primary aerospace applications has been hindered due in part to their characteristic anisotropic mechanical and fracture behaviors. The Air Force recently developed two isotropic Al-Li-Cu-X alloys with 2.1 wt pct Li and 1.8 wt pct Li designated AF/C-489 and AF/C-458, respectively. The elongation at peak strength was less than the required 5 pct for the 2.1 wt pct Li variant but greater than 10 pct for the 1.8 wt pct Li alloy. The objectives of our investigations were to first identify the mechanisms for the large difference in ductility between the AF/C-489 and AF/C-458 alloys and then to develop an aging schedule to optimize the microstructure for high ductility and strength levels. Duplex and triple aging practices were designed to minimize grain boundary precipitation while encouraging matrix precipitation of the T_1 (Al_2CuLi) strengthening phase. Certain duplex aged conditions for the AF/C-489 alloy showed significant increases in ductility by as much as 85 pct with a small decrease of only 6.5 and 2.5 pct in yield and ultimate tensile strength, respectively. However, no significant variations were found through either duplex or triple aging practices for the AF/C-458 alloy, thus, indicating a very large processing window. Grain size and δ' (Al_3Li) volume fraction were determined to be the major cause for the differences in the mechanical properties of the two alloys.

I. INTRODUCTION

IN this era of streamlined economics for the aerospace industry, weight reduction of aerospace vehicles is best achieved through decreasing the density of the aircraft's structural materials. For aluminum alloys, lithium is added to reduce the alloy's density with the added benefit of increasing the alloy's modulus. In fact, the addition of 2 wt pct lithium can reduce the density of aluminum by 6 pct and increase the modulus by 12 pct,[1] thus, decreasing the system weight and operational costs while increasing the intrinsic alloy strength. Nevertheless, extensive implementation of aluminum-lithium alloys into primary aerospace structures has been hindered, in part, due to their characteristic anisotropic mechanical behavior,[2] unusual fracture behavior,[3] poor short transverse properties,[4] and higher production costs.

A recent Air Force sponsored program focused on an effort to develop an aluminum-lithium alloy containing greater than 2 wt pct lithium that possessed significantly reduced anisotropic properties compared to those currently available.[5] Starke suggested that an intermediate recrystallization anneal be introduced between rolling stages to reduce the sharp textures caused by the rolling and thereby decrease the alloy's anisotropy.[6] This added step proved highly successful as the anisotropy of both the modulus and yield strength were reduced significantly from 20 to 25 pct for current aluminum-lithium alloys to less than 10 pct for the Air Force alloy. The subsequent Air Force alloy was designated. AF/C-489 with a nominal composition of Al-2.7 wt pct Cu-2.1 wt pct Li-0.6 wt pct Zn-0.3 wt pct Mn-0.3 wt pct Mg-0.05 wt pct Zr. Unfortunately, the elongation at peak strength was lower than the acceptable level of 5 pct for aerospace applications.

As a result of this research, the Air Force and ALCOA (Alcoa Center, PA) developed a derivative of AF/C-489 with 1.8 wt pct Li and 0.09 wt pct Zn, designated AF/C-458, with the nominal composition of Al-2.7 wt pct Cu-1.8 wt pct Li-0.6 wt pct Zn-0.3 wt pct Mn-0.3 wt pct Mg-0.09 wt pct Zr. This AF/C-458 variant possessed much higher elongations, more than double the acceptable limit, while also maintaining similar isotropic mechanical properties. Therefore, the objectives of our investigations were to first identify the mechanisms for the large difference in ductility between the AF/C-489 and AF/C-458 alloys and then to develop an aging schedule to optimize the microstructure for high ductility and strength levels.

II. BACKGROUND

Low ductility resulting from low energy intergranular fracture in Al-Li-Cu-X alloys has been attributed to a number of factors that include tramp elements,[7,8,9] constituent particles,[10,11,12] strain localization in the matrix,[13–16] grain structure,[16] crystallographic texture,[17] and grain boundary precipitates[18] with their corresponding precipitate-free zones[19] (PFZs). Tramp impurity elements such as Na, K, Ca, H, and S have been shown to segregate to grain boundaries, thereby weakening the boundary and leading to low energy intergranular fracture.[7,8,9] The Fe and Si impurities, on the other hand, lead to the formation of coarse constituent particles during the casting process, which have been shown to drastically degrade the fracture toughness of various aluminum alloys.[10] Accordingly, both AF/C-489 and AF/C-458 alloys were designed to minimize the concentrations of both

A.A. CSONTOS, Graduate Student, and E.A. STARKE, Jr., University Professor and Oglesby Professor of Materials Science and Engineering, are with the Department of Materials Science and Engineering, University of Virginia, Charlottesville, VA 22903.

Manuscript submitted September 17, 1999.

the tramp elements (Na, K, Ca, H, and S) and constituent particle forming elements (Si, Fe) to well below those that have been shown to cause low ductility.

Apart from chemical inhomogeneities, strain localization in the matrix has been shown to be a major cause for low ductility in high-purity Al-Li-Cu-X alloys, *e.g.*, AF/C-489 and AF/C-458. This strain localization occurs by two distinctly different mechanisms: (1) cutting of shearable precipitates such as δ' (Al_3Li) and (2) the preferential deformation of the softer PFZs. Binary Al-Li alloys with greater than 5.8 at. pct Li or 1.6 wt pct Li and complex Al-Li-Cu-X alloys, *e.g.*, AF/C-489 and AF/C-458, with sufficient Li concentrations homogeneously precipitate the ordered, coherent, spherical, and shearable strengthening precipitate, δ'.[13] The concomitant shearing of these δ' precipitates with each passing dislocation effectively softens the active slip plane, resulting in coarse planar slip and the formation of intense slip bands, which impinge on grain boundaries, thus causing premature intergranular fracture.

Softer PFZs form in the matrix adjacent to grain boundaries by two different mechanisms: (1) solute depletion and (2) vacancy depletion. In either case, the PFZ is significantly softer than the precipitate hardened matrix, resulting in slip localization in the PFZ and at the grain boundary triple junctions, which also leads to premature intergranular fracture. Furthermore, the heterogeneous precipitation of coarse grain boundary particles such as T_2 (Al_6Li_3Cu)[20] and T_X ($Al_XLi_YCu_Z$)[21] has been shown to lead to intergranular fracture due to microvoid nucleation and coalescence.

Minimizing strain localization in the matrix during deformation is critical to increasing the ductility and improving the fracture behavior of Al-Li-X alloys. Slip length or the measured distance between concurrent nonsheared microstructural features, *e.g.*, incoherent precipitates, dispersoids, grain boundaries, *etc.*, in the slip plane is a critical microstructural parameter, which many fracture models[22–27] utilize to accurately describe the degree of strain localization in an Al-Li-X alloy. In other words, microstructures with large slip lengths in Al-Li alloys encourage planar slip, while short slip lengths change the slip characteristics from planar to wavy glide, thus, homogenizing deformation and reducing stress concentrations, which lead to premature fracture.

Microstructural features such as the grain size, dispersoid size, and morphology, crystallographic texture, and heterogeneous precipitation of strengthening particles all significantly affect the slip length and, thus, the fracture behavior of these Al-Li-Cu-X alloys. For example, grain size has been shown to vary inversely to the true fracture strain ($L^{-1} \sim \varepsilon_f$) of a Ti-Al binary alloy with shearable, coherent, spherical Ti_3Al precipitates very similar to δ' in Al-Li alloys.[16] Consequently, dispersoid-forming elements such as Mn and Zr are added to Al-Li-Cu-X alloys, *i.e.*, AF/C-489 and AF/C-458, to control the grain size and structure.

The Mn additions form the incoherent, nonshearable, cigar-shaped $Al_{20}Mn_3Cu_2$[7] and Al_6Mn[28] dispersoid particles, which generally have dimensions less than 0.5 μm in diameter and 1.0 μm in length for high-purity Al-Li-Cu-X alloys. Starke and Lin[29] and Walsh[30] *et al.* showed that both coarse primary and submicrometer Mn dispersoids nucleate voids and thereby encourage the fracture process; however, their results also demonstrate that the maximum ductility of an Al-Cu-Mg-Zr alloy contained a 0.31 wt pct addition of Mn. Their void nucleation and growth data coupled with their microstructural analysis suggests that the 0.31 wt pct addition of Mn produced sufficient submicrometer sized dispersoids to homogenize slip without forming the large, coarse, primary Mn-rich particles, which were shown to decrease the ductility.

The Zr additions are designed to form β' (Al_3Zr) dispersoids, which act to greatly inhibit recrystallization during ingot breakdown and hot rolling. Nevertheless, the Zr additions strongly aid the formation of a pancake grain structure and an intense crystallographic texture. Consequently, this strong texture can produce adjacent grains and subgrains with low misorientations, thereby, allowing glissile dislocations to penetrate their boundaries, which effectively increases the grain size and, thus, the slip length. To reduce the intense crystallographic texture associated with Zr additions, methods such as a cross-rolling procedure as well as an intermediate recrystallization anneal between rolling steps have been shown to significantly reduce the texture and, more interestingly, the anisotropy of certain Al-Li-Cu-X alloys.[31,32,33]

Nevertheless, the most effective method to improve the ductility of Al-Li alloys is to develop a microstructure that contains various nonshearable precipitates in the matrix, which act to homogenize slip.[15,30,33] Maximizing matrix precipitation and minimizing coarse grain boundary formations of nonshearable metastable and equilibrium strengthening phases is critical in order to reduce the slip length and increase ductility. For Al-Li-Cu alloys, a preage stretch coupled with a low-/high-temperature duplex aging schedule has been shown to substantially increase the ductility and fracture toughness of various Al-Li alloys.[34–38] The low-temperature aging maximizes the driving force for nucleation, while the preage stretch introduces dislocations as competitive nucleation sites to grain boundaries. In complex Al-Li-Cu-X alloys, a more substantial stretch is normally employed, since T_1 nucleation is greatly influenced by dislocation jogs.[39,40] However, in order to determine the optimal aging practices for both AF/C-489 and AF/C-458 alloys, a detailed knowledge of the precipitation reaction of the metastable strengthening phases, *i.e.*, θ', T_1, and δ', is essential.

III. EXPERIMENTAL PROCEDURES

Air Force Research Labs and ALCOA provided both the 0.5-in.-thick 2.1 wt pct Li AF/C-489 and 0.75-in.-thick 1.8 wt pct Li AF/C-458 alloys that were utilized for this investigation. Both alloy ingots were direct chill cast, stress relieved, homogenized, hot rolled, annealed at 540 °C for 4 hours, and then slow cooled before being hot rolled again. This was followed by solution annealing at 540 °C for 1 hour and an immediate water quench. Finally, a 6 pct preage stretch was conducted within 8 hours of quenching to avoid natural aging effects, which can influence the homogeneity of the dislocation substructure and, thus, the heterogeneous precipitation of the metastable strengthening phases. For both AF/C-489 and AF/C-458 alloys, a 6 pct preage stretch was determined to provide the greatest matrix T_1 precipitation with the least amount of stretch.[41] Therefore, the T36 temper for both the AF/C-489 and AF/C-458 alloys serves as the "as-received" material from which all aging studies were carried out for this investigation.

All aging studies were conducted in forced air furnaces with temperature fluctuations less than ±2 °C and immediately water quenched. Continuous differential scanning calorimetry studies of the as-received T36 samples were accomplished with a PERKIN-ELMER* Series 7 model differential scanning calorimeter with a heating rate of 3 °C/min. Tensile samples were machined into cylindrical and dog-bone tensile bars conforming to ASTM E-8 substandard size regulations and tested utilizing the screw driven Sintech 10/GL MTS system with a strain rate of 3 mm per minute. Optical samples were cut from the longitudinal (L), long transverse (LT), and short transverse (ST) directions and then polished down to 0.05-μm colloidal silica solution and then etched with Keller's agent. Digital scanning electron microscopy fractographs were acquired through the use of a DSM982 Gemini field-emission scanning electron microscope (SEM) operating at 10 kV equipped with dual backscatter electron detectors, one perpendicular and the other at 45 deg to the surface.

*PERKIN-ELMER is a trademark of Perkin-Elmer Physical Electronics, Eden Prairie, MN.

Transmission electron microscopy (TEM) samples were cut from the grip section for microstructural analysis and the gage section for slip behavior investigations. The cut wafers were then mechanically thinned to ~150-μm thickness, punched into 3-mm disks, and electropolished in a Tenupol twin-jet electropolisher at 11 V for the AF/C-458 alloy and 8 V for the AF/C-489 alloy at a flow rate of 3 and photosensitivity of 9. A 3.5:1 methanol: nitric acid solution was utilized as the electrolyte after being cooled to −25 °C. Conventional TEM was accomplished using a JEOL* 2000FX transmission electron microscope at 200 kV, while high resolution TEM was completed with the JEOL 4000 high resolution electron microscope (HREM) operating at 400 kV. Centered dark-field (CDF) and bright-field (BF) techniques were used to observe the precipitate size and distribution. Stereological quantification of the T_1 lath and θ'' plate shaped precipitates in thin TEM foils was completed through a statistical analysis[42] to overcome thin foil effects, which underestimates the diameters and volume fractions of the T_1 and θ'' precipitates from two-dimensional TEM micrographs.[43] Furthermore, foil thickness was determined by the well-established convergent-beam technique[44] and weak-beam dark-field (WBDF) was utilized with a large, positive deviation parameter to examine the dislocation particle interactions.

*JEOL is a trademark of Japan Electron Optics Ltd., Tokyo.

IV. RESULTS AND DISCUSSION

A. *Grain Structure, Microstructure, and Properties of Both T36 and T4 Alloys*

The grain and subgrain structures of both T36 as-received AF/C-489 and AF/C-458 plates are demonstrated qualitatively by the optical micrographs in Figures 1(a) through (d) and quantitatively in Table I. Clearly, the 0.5-in.-thick AF/C-489 plate contains a much larger average grain size in all three planes, *i.e.*, rolling (LT), longitudinal (LS), and transverse (ST), as compared to the 0.75-in.-thick AF/C-458 plate. Quantitatively, the AF/C-458 grains possessed an aspect ratio roughly twice that of the AF/C-489 plate, while the number of grains counted over a 500-mm circumference were from ~2.5 to 3 times greater in the AF/C-458 alloy than in the AF/C-489 plate.

Low-magnification BF TEM was conducted for both AF/C-489 and AF/C-458 to ensure that both alloys were received in an unrecrystallized condition. The TEM micrographs in Figures 1(c) and (d) clearly demonstrate the unrecrystallized microstructures for both as-received T36 alloys as seen by the approximate 5- to 10-μm subgrain size. The mechanical properties of both T36 alloys were quite similar except for the 40 MPa variation in yield strength, which may be associated with the grain size difference or other microstructural features such as natural aging.

Microstructural analysis of both T36 alloys, as seen in Figures 2(a) through (d), demonstrates the natural aging of the matrix δ' with the characteristic dislocation structure resulting from the 6 pct preage stretch. Furthermore, Figure 3 clearly shows the large strengthening effect that δ' natural aging has on the AF/C-458 T4 alloy. Due to this natural aging of the shearable δ', Alcoa stretched both alloy plates within the first 8 hours after quenching,[6] albeit, still too late as a substantial δ' volume fraction had already precipitated. Ideally, the preage stretch should be accomplished within the first 3 hours of quenching to overcome the associated problems with the naturally aged δ', *i.e.*, nonuniform deformation due to planar slip. The resulting nonuniform dislocation structure could then affect the competitive precipitation kinetics of the metastable T_1 strengthening phase and, thus, the mechanical properties of the alloy.

B. *Microstructural Evolution and Mechanical Properties of Both Single Aged T86 Alloys*

Designing an artificial aging schedule subsequent to the 6 pct preage stretch required knowledge of the precipitation and strengthening response of both the AF/C-458 and AF/C-489 alloys as a function of time and temperature. Therefore, differential scanning calorimetry (DSC) and TEM studies were conducted to fully characterize the precipitation response from the T36 temper for both alloys. Bright-field TEM and diffraction pattern analysis of θ'' streaking along $g = (200)_\alpha/b = [001]_\alpha$ and T_1 streaking-along $g = (111)_\alpha/b = [011]_\alpha$ indicated that the onset of θ'' and T_1 precipitation occurred between 90 °C to 95 °C and 120 °C to 125 °C, respectively, for both AF/C-458 and AF/C-489 alloys.

In order to evaluate the strengthening effectiveness of various aging routes, baseline hardness data were acquired to determine the various single-aged schedules. Figure 4 demonstrates the variation of the Rockwell B hardness values for both the AF/C-458 and AF/C-489 alloys as a function of single aging time at 100 °C, 125 °C, 130 °C, 135 °C, and 150 °C. Note that the slopes increase slowly and relatively linearly for the 100 °C and 125 °C ages, where θ'' is the main strengthening precipitate. However, the strengthening rates for the 130 °C and 135 °C treatments increase more rapidly through the first day of aging and then decrease to similar rates as the 125 °C curves. This initial rapid strengthening may be due to initial T_1 nucleation and early growth, which then slows at such low temperatures, *i.e.*, 10 °C, above the T_1 onset temperature. The 150 °C hardness curves are quite different, however, when compared to the other lower temperature plots. The slopes of these curves are

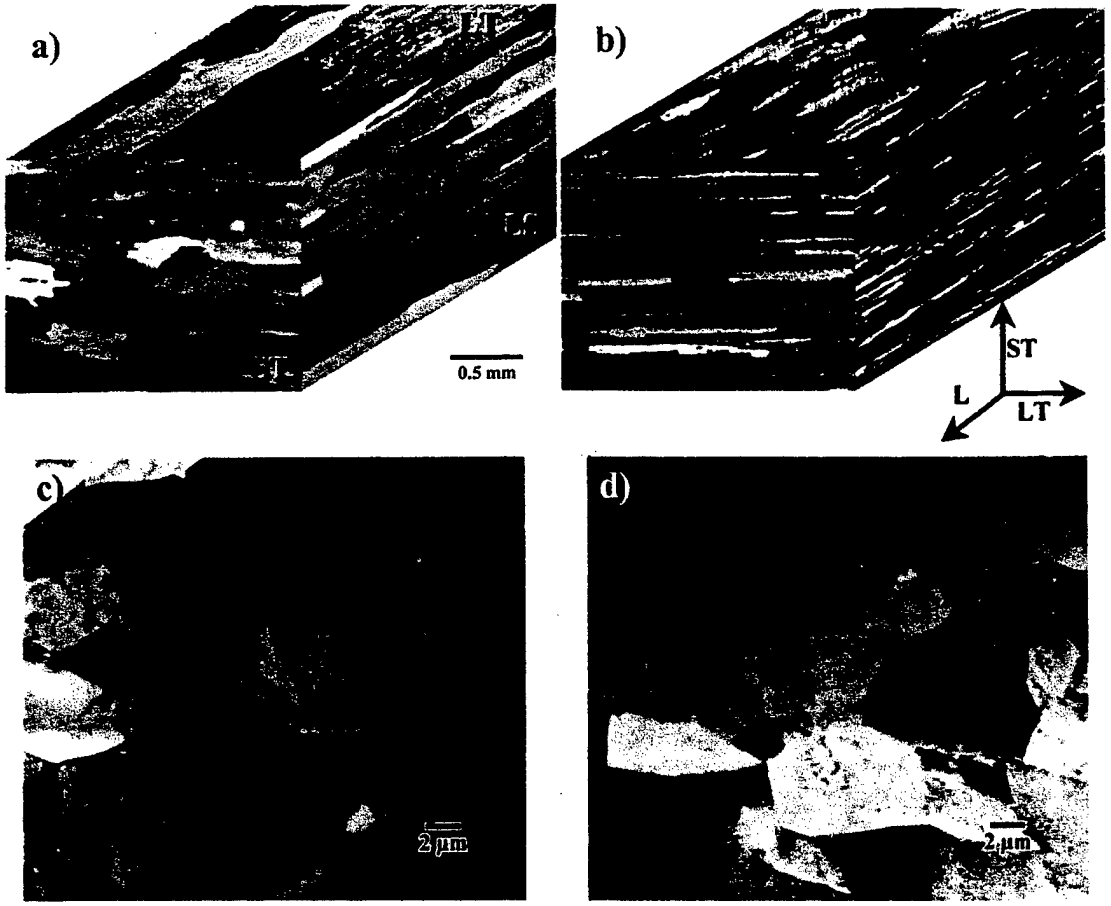

Fig. 1—(*a*) and (*b*) Optical and (*c*) (*d*) BF TEM micrographs illustrating the pancake grain structure and unrecrystallized subgrain structure for (a) and (c) AF/C-489 and (b) and (d) AF/C-458 alloys.

Table I. Mechanical Properties, Grain Size, and Aspect Ratio Data for Both Alloys

Yield Strength (MPa)	Ultimate Strength (MPa)	ε_f Fracture Strain	LT Aspect Ratio	Number of Grains/ 500 mm	LS Aspect Ratio	Number of Grains/ 500 mm	ST Aspect Ratio	Number of Grains/ 500 mm
AF/C-489 0.50-in.-Thick Plate								
254	342	17.3 pct	3.4	18	19.7	75	10.1	83
AF/C-458 0.75-in.-Thick Plate								
291	351	17.7 pct	6.7	42.2	34.2	228.5	24.6	261.3

substantially higher than the lower temperature counterparts, which suggests that the T_1 nucleation and growth rates are much higher than at the lower temperatures. These results indicate that the 150 °C single age practice provides a good combination of both high matrix T_1 nucleation and growth rates, *i.e.*, near the nose of the time, temperature, and transformation curve.

The next step in determining a baseline 150 °C single aging schedule was to develop the best combination of strength to ductility as a function of the aging time at 150 °C. Figures 5 and 6 demonstrate the tensile properties as a function of aging time at 150 °C for the AF/C-458 alloy in both the longitudinal and transverse directions, respectively. Note that the best combination of strength to ductility from both the longitudinal and transverse data was in the slightly underaged condition, which was expected, at 150 °C for 24 hours. Also, note that the anisotropy between directions was determined to be, on average, less than 7 and 5 pct for the yield and ultimate tensile strengths, respectively, while the elongations were on average greater than twice the acceptable level of 5 pct. Therefore, this single age of 150 °C for 24 hours was utilized for all initial baseline mechanical property examinations.

Microstructural features of the baseline 150 °C 24 hours single age for both the AF/C-458 and AF/C-489 alloys are shown in Figures 7 and 8. Qualitatively, the BF and CDF TEM micrographs clearly show that T_1, θ'' engloved with δ', and δ' are the major strengthening precipitates in both alloys at the 150 °C 24 hour single age. Matrix T_1 precipitation is high in both alloys and, as seen in Figures 7(c) and 8(c), two typical variants of grain boundary T_1 are apparent. Grain boundary puckering and oriented T_1 are two distinct

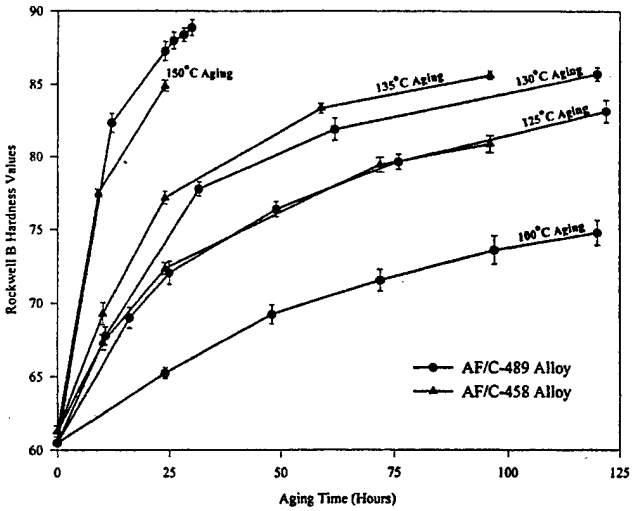

Fig. 4—Rockwell B hardness *vs* aging time.

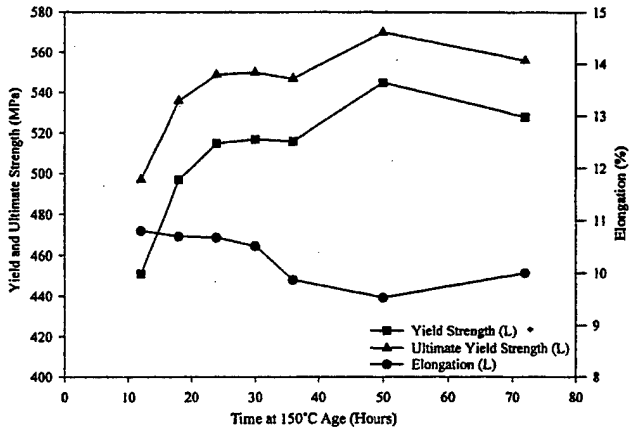

Fig. 5—Longitudinal tensile mechanical properties data for the AF/C-458 alloy.

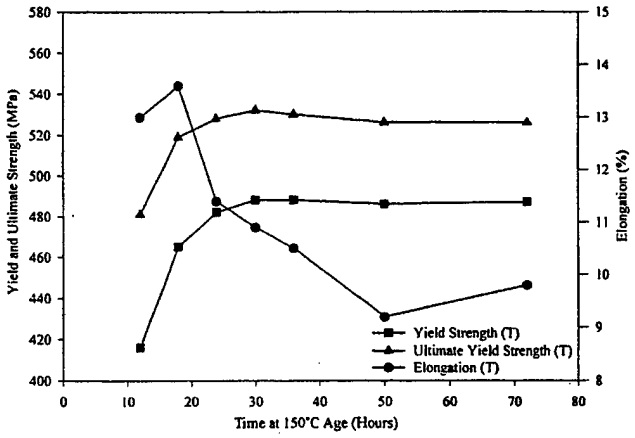

Fig. 6—Transverse tensile mechanical properties data for the AF/C-458 alloy.

variants of typical grain boundary precipitates found in both alloys. Grain boundary puckered T_1 was found to be more prevalent, as oriented grain boundary T_1 was more unusual since most grain boundaries were found not to be oriented along a specific (111) habit plane.

C. *Microstructure and Mechanical Properties of Multiple Aged T86 Alloys*

Since grain boundary T_1 was observed in both 150 °C 24 hour aged samples, duplex and triple aging studies were conducted in an effort to minimize grain boundary T_1 and maximize matrix T_1 precipitation, thereby, increasing the ductility of these alloys. A preage stretch coupled with a low-/high-temperature duplex aging schedule has been shown to substantially increase the ductility and fracture toughness of various Al-Li alloys.[34–38] The low-temperature age above 120 °C was designed to maximize the driving force for matrix T_1 nucleation on dislocations and jogs followed by a higher temperature age to promote subsequent matrix T_1 growth. Furthermore, other duplex and triple aging studies were designed to tie up the Cu atoms in the matrix through the precipitation of a fine θ'' dispersion at temperatures between 95 °C to 120 °C. The higher temperatures of the subsequent steps would then precipitate the matrix T_1, and since the Cu atoms were tied up in the matrix, the grain boundary T_1 variant would be minimized. The hope of these various aging routes was to increase the matrix T_1 density, which would, in turn, reduce the slip length and strain localization and promote greater ductility.

Figures 9(a) and (b) show the results of the various duplex and triple aging practices that were designed with the DSC and TEM data. The duplex aging of the AF/C-489 alloy resulted in promising increases in strain to fracture above the required 5 pct with only small losses in strength. In fact, as seen in Figures 10(a) and (b), the best duplex aging results of the AF/C-489 alloy reported significant increases in ductility by as much as 85 pct with a small decrease of only 6.5 and 2.5 pct in yield and ultimate tensile strength, respectively. Nevertheless, neither the double or triple aging practices designed for the AF/C-458 alloy proved effective in substantially altering the yield strength, ultimate tensile strength, and ductility. This point suggests that a very large processing window exists for the AF/C-458 alloy even with the wide variations in aging temperatures and time to achieve comparable strength levels to the 150 °C single age. Figures 10(a) and (b) also demonstrate the isotropic nature of the mechanical properties between the longitudinal and transverse directions for the AF/C-458 and, to a lesser degree, the AF/C-489 alloys. In fact, our results indicate the anisotropy difference to be less than 5 pct for the AF/C-458 alloy, which is quite unique for Al-Li-Cu-X alloys.

To examine the effect of the precipitate type, density, and size on the mechanical properties, quantitative microstructural analysis of the major precipitates is shown in Table II for both the single and duplex aged conditions corresponding to Figures 10(a) and (b). The major difference between the two alloys in the single aged 150 °C 24 hour condition was the ~3 pct higher δ' volume percent for the AF/C-489 alloy, while the duplex aged results showed that variations in the competitive precipitation of T_1 and θ'' were also evident for the AF/C-489 alloy. For the AF/C-458 alloy, the T_1 and θ'' volume percents and, correspondingly, the mechanical properties remain very similar for the single and duplex aged data, while only the number densities increase and mean diameter decrease as anticipated by the duplex aging theory.

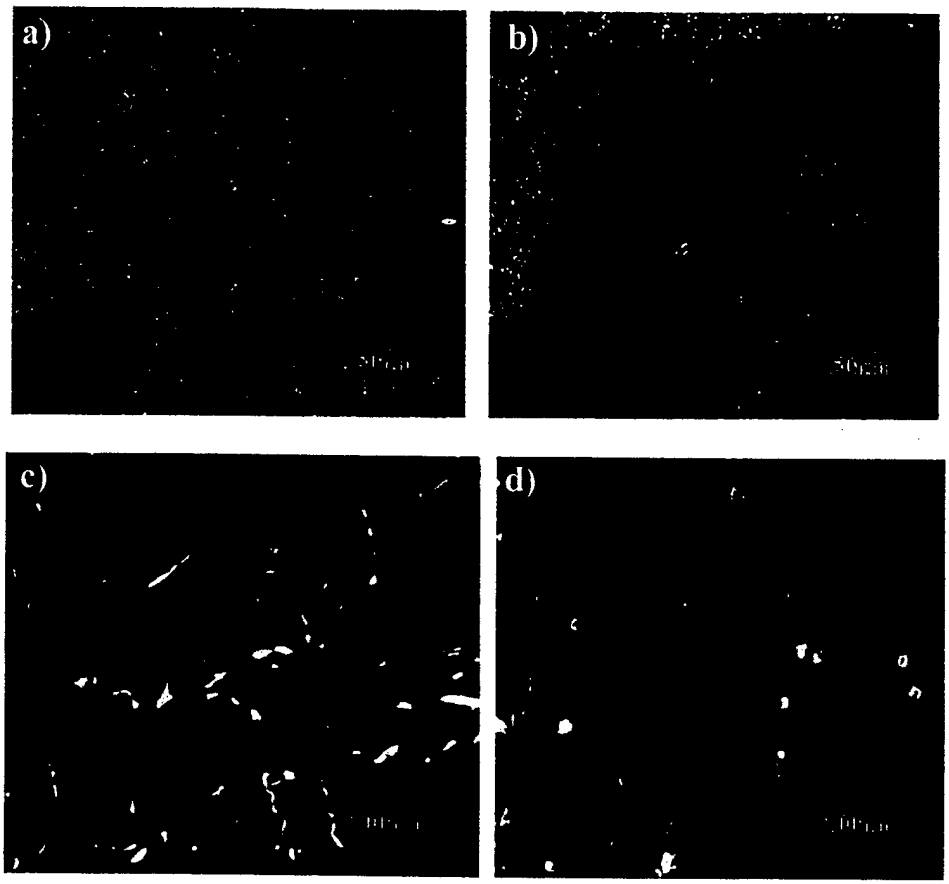

Fig. 2—CDF micrographs of both T36(*a*) AF/C-489 and (*b*) AF/C-458 alloys after ~2 years of δ' natural aging after solutionizing at 540 °C for 1 h, $\mathbf{b} = [011]_{\alpha}$, $g = (100)_{\delta'}$. WBDF TEM of both T36 (*c*) AF/C-489 and (*d*) AF/C-458 alloys indicating the dislocation structure in the matrix, $\mathbf{b} = [110]_{\alpha}$, g, $3g = (111)$.

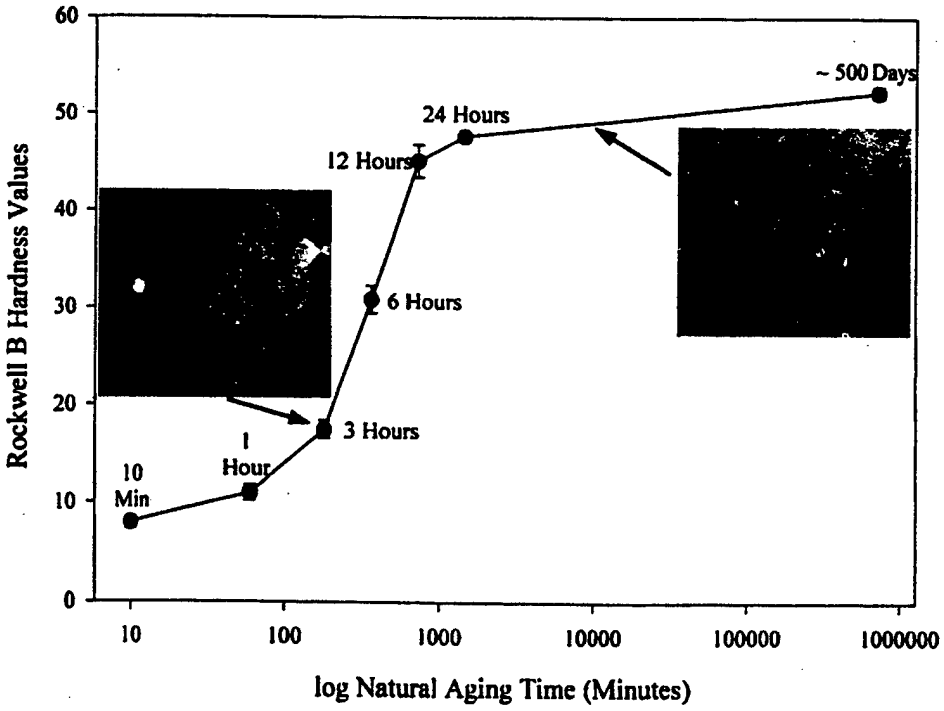

Fig. 3—Rockwell B hardness *vs* room temperature aging time for the AF/C-458 T4 alloy following a solution treatment at 540 °C for 1 h and water quenching, demonstrating the strengthening effect of δ' precipitation.

Fig. 7—AF/C-458 150 °C 24 h micrographs: (*a*) CDF image showing δ' and θ'' engloved with δ' (θ''/δ'), $\mathbf{b} = [011]_\alpha$, $g = (100)_{\delta'}$; (*b*) BF indicating θ'' and matrix and grain boundary puckering T_1, $\mathbf{b} = [110]_\alpha$; (*c*) CDF micrograph showing matrix and grain boundary puckering T_1, $\mathbf{b} = [110]_\alpha$, $g = \frac{1}{2}(111)_\alpha$.

Fig. 8—AF/C-489 150 °C 24 h micrographs: (*a*) CDF image showing δ' and θ'' engloved with δ' (θ''/δ'), $\mathbf{b} = [011]_\alpha$, $g = (100)_{\delta'}$; (*b*) BF indicating θ'' and matrix and grain boundary puckering T_1, $\mathbf{b} = [110]_\alpha$; (*c*) CDF micrograph showing matrix and grain boundary puckering T_1, $\mathbf{b} = [110]_\alpha$, $g = \frac{1}{2}(111)_\alpha$.

As with the mechanical properties, the AF/C-489 precipitation behavior varied significantly with the added preage step in the duplex anneal. The T_1 volume percents decreased by nearly half, while the θ'' volume percents and number densities increased significantly with the added low-temperature age. These data suggest that the variation in tensile properties between the single and duplex aged AF/C-489 alloy depends upon which strengthening precipitate, *i.e.*, weaker θ'' *vs* stronger T_1, is dominant in the final microstructure.

Nevertheless, as seen in Figures 11(a) through (f), dark-field TEM indicates the presence of fine grain boundary T_1 along subgrains with less than 5 deg misorientation in both the AF/C-489 and AF/C-458 single and duplex aged samples. Coarse grain boundary T_1 and its associated PFZs were not observed in any of the single, duplex, and triple aged samples at or below 150 °C. Therefore, the tensile data coupled with the TEM analysis seem to indicate that the fine grain boundary T_1 precipitation is not the limiting parameter that affects the ductility of these alloys.

D. *Analysis of Slip Behaviors for δ', θ'', and T_1 and SEM Fractography*

Whether δ', θ'', and/or T_1 shear with mobile dislocations is a major factor that leads to strain localization and, thus, premature intergranular fracture. Clear evidence of sheared δ' and T_1 and the subsequent strain localization in the form of shear bands are shown in Figures 12(a) through (d) and 13(a) through (d) for both alloys aged at 150 °C 24 hours and plastically strained to 2 pct. The TEM investigations of the strained gage sections from all single and duplex aged tensile samples confirmed the formation of intense shear bands. The TEM analysis further showed that the cigar-shaped $Al_{20}Cu_2Mn_3$ dispersoids were not sheared, but that the T_1 adjacent to these dispersoids was still sheared.

The SEM fractography results of the fractured tensile samples, as seen in Figures 14(a) through (d) and 15(a) and (b), clearly demonstrate the flat and intergranular nature of the AF/C-489 single aged longitudinal and transverse fractured tensile samples as well as the duplex aged transverse fractured tensile samples. Conversely, the longitudinal 100 °C (not pictured), 120 °C, and 130 °C duplex aged tensile samples fractured close to 45 deg, indicating more high energy transgranular shearing, which is favorable for higher ductility. However, large regions of low energy intergranular fractured grains were still evident along with smaller areas of transgranular shearing, dimpled rupture, and microvoid coalescence (MVC) for these duplex aged AF/C-489 fractured tensile samples.

In contrast, as seen in Figures 14(a) and (c), all of the longitudinal and transverse AF/C-458 tensile samples fractured either with the classic ductile cup and cone or slant 45 deg fracture, thus, possibly indicating more of a transgranular shear component and less intergranular fracture. Figure 15(a) confirms this point as the fractured grains were much cleaner, indicating more high energy transgranular shearing and grain boundary sliding with regions of high energy dimpled rupture and MVC. Also note Figure 15(b) for a similarly aged AF/C-489 alloy, which shows large slip offsets characteristic of strain localization or slip concentrations impinging a grain boundary. These large slip offsets are clearly absent in Figure 15(a) for the similarly aged AF/C-458 alloy, which suggests that strain localization played a

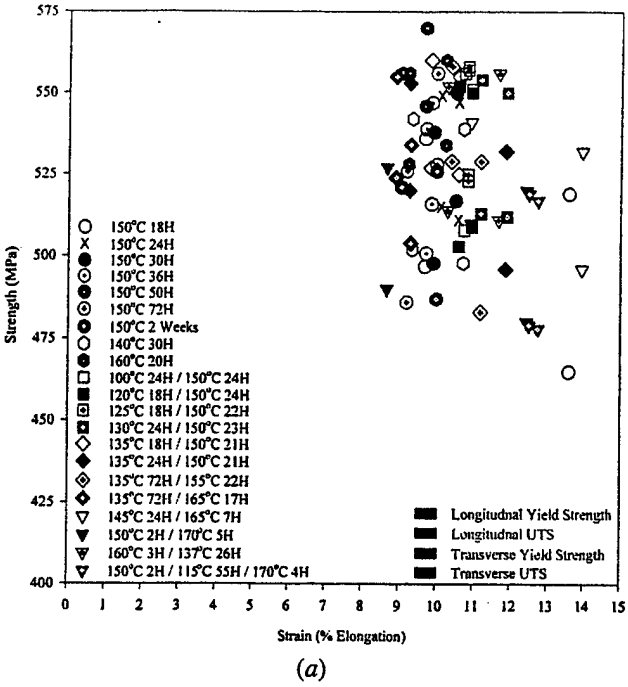

(*a*)

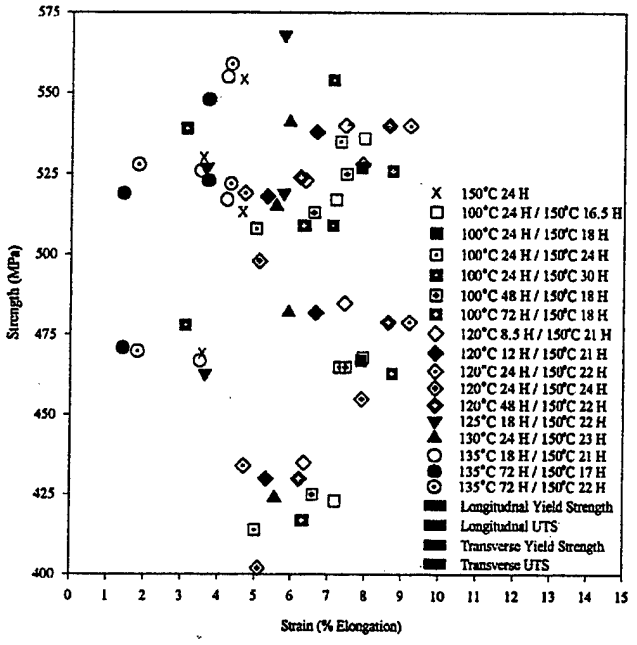

(*b*)

Fig. 9—(*a*) AF/C-458 and (*b*) AF/C-489 strength *vs* strain for various aging treatments.

key role in the fracture process and, thus, the low ductility of the AF/C-489 alloy in comparison to the AF/C-458 alloy. Finally, these SEM fractographs also corroborate the optical microscopy results in Figure 1, which showed the substantial grain size variation between the AF/C-458 and AF/C-489 alloys.

E. *Deformation, Fracture, and Slip Distribution*

Mechanistically, strain localization in Al-Li alloys with δ' has been shown to relate to slip plane softening after the

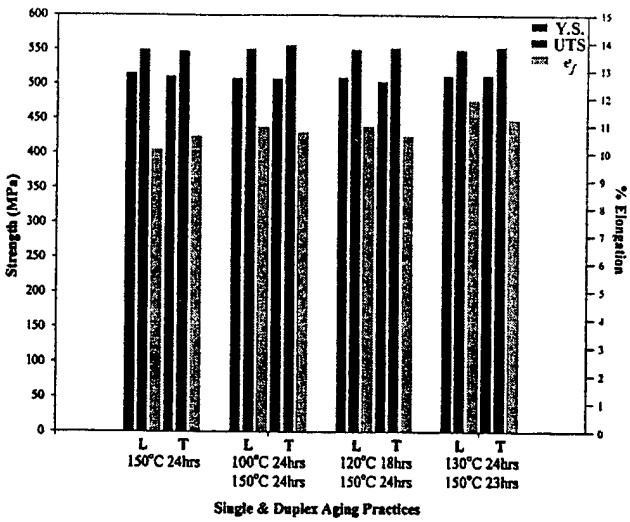

(*a*)

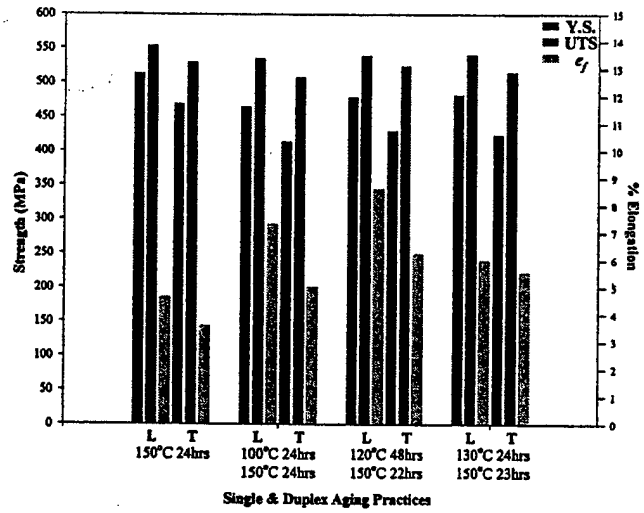

(*b*)

Fig. 10—(*a*) AF/C-458 and (*b*) AF/C-489 mechanical properties for the 150 °C 24 h single age and duplex aged results.

initial dislocations shear the precipitate followed by slip plane hardening due to the back stresses associated with the pileup at a major deformation barrier. Hence, Duva *et al.*[22] proposed a method to quantify strain localization as the number of dislocations expected in a pileup since this is measure of a microstructure's ability to deform by planar slip:

$$N = f^{1/2} r^{1/2} L \frac{C_p}{C_B \mathbf{b}} \qquad [1]$$

where N is the number of dislocations, f the volume fraction of δ', r the δ' radius, L the slip length, **b** the burgers vector, C_p the constant that is related to the antiphase boundary energy of δ', and C_B the constant that depends on the matrix shear modulus. Blankenship *et al.*[23] combined these slip intensity calculations with estimates of the critical particle size for the shearing-to-looping transition of S′ phase and predicted the slip distribution in complex Al-Li-Cu-X alloys.

By utilizing these relationships, Cassada *et al.*[15] and Blankenship and Starke[34] were able to develop microstructures that reduced the slip length and strain localization by

Table II. Quantitative Precipitate Data for Both Single and Duplex Aged AF/C-458 and AF/C-489 Alloys Corresponding to the Data Shown in Figures 10(a) and (b)

Alloy/ Aging Practice	T_1 Vol Pct	T_1 Number Density $(\mu m^{-3})^{-1}$	T_1 Mean Diameter (nm)	θ'' Vol Pct	θ'' Number Density $(\mu m^{-3})^{-1}$	θ'' Mean Diameter (nm)	δ' Vol Pct	δ' Mean Diameter (nm)
AF/C-458								
150 °C 24 hour	3.2 pct	7,690	58	0.23 pct	1,411	45	6.3 pct	7.8
100 °C 24 hour								
150 °C 24 hour	3.0 pct	8,860	52	0.31 pct	10,330	19	5.7 pct	7.7
120 °C 18 hour								
150 °C 24 hour	3.1 pct	10,920	48	0.24 pct	11,120	17	5.2 pct	7.8
130 °C 24 hour								
150 °C 23 hour	3.0 pct	11,000	44	0.49 pct	12,900	22	5.8 pct	7.7
AF/C-489								
150 °C 24 hour	2.9 pct	7,440	57	0.26 pct	4,200	29	9.1 pct	7.8
100 °C 24 hour								
150 °C 24 hour	1.2 pct	5,550	43	1.38 pct	65,430	16	8.8 pct	7.6
120 °C 48 hour								
150 °C 22 hour	1.7 pct	7,700	41	1.03 pct	28,060	22	8.9 pct	7.7
130 °C 24 hour								
150 °C 23 hour	1.7 pct	7,660	42	1.06 pct	28,400	22	9.3 pct	7.7

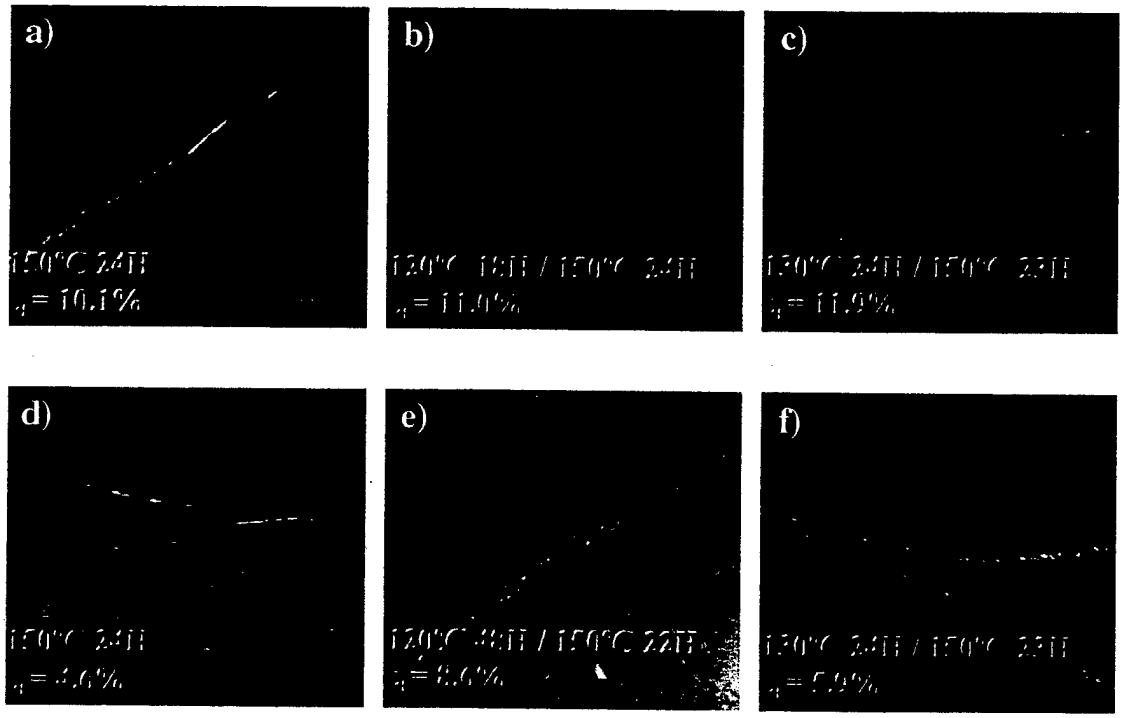

Fig. 11—CDF TEM micrographs demonstrating the fine subgrain boundary T_1, $\mathbf{b} = [110]_\alpha$, $g = \frac{1}{2}(111)_\alpha$ for (*a*) through (*c*) AF/C-458 and (*d*) through (*f*) AF/C-489 alloys with the respective aging schedules denoted on the micrographs.

homogenizing slip. Cassada added Ge to an Al-Li binary alloy to precipitate out Ge rods ~20 nm in length, which effectively homogenized slip. The Ge particles, thus, reduced the slip length from the grain size to the interparticle spacings of the Ge precipitates, which changed the slip distribution from coarse planar to homogeneous slip. On the other hand, Blankenship developed a duplex age for AA8090, which reverted most of the δ' and continued the S′ growth. This age proved highly successful as the fracture toughness of the alloy was dramatically increased since planar slip was reduced due to the reduction of δ' volume fraction and the larger S′ particles.

Our investigation indicates that duplex aging had little effect on the AF/C-458 ductility, while having nominal success for the AF/C-489 alloy. To understand the differences between the duplex age results, we must consider the governing parameters in Eq. [1]. The quantitative TEM data showed that the δ' volume fraction and diameter remained relatively constant between the single and duplex aging practices, *i.e.*, ~6 pct and ~8 nm for AF/C-458 and ~9 pct and ~8 nm for AF/C-489, respectively. However, δ' volume fraction was on average 3 vol pct higher in the AF/C-489 alloy as compared to the AF/C-458 alloy with similar heat treatments. Our results also indicate that the duplex aging of the AF/

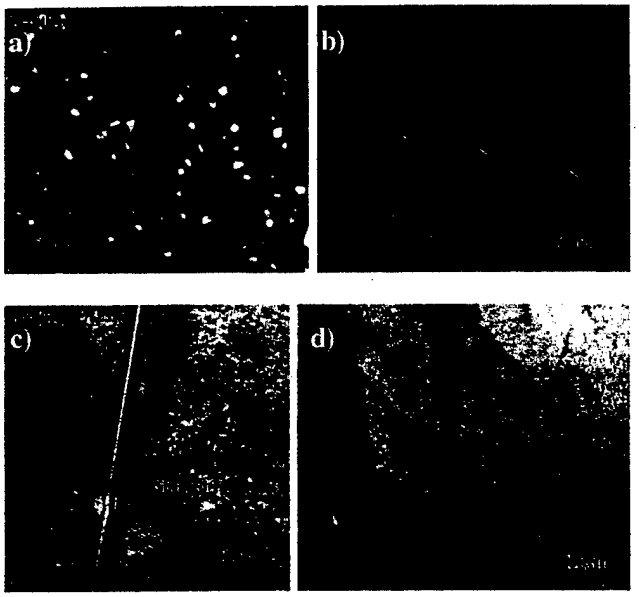

Fig. 12—AF/C-458 150 °C 24 h 2 pct plastic strained micrographs: (*a*) CDF image showing sheared δ' (arrows), $\mathbf{b} = [110]_\alpha$, $g = (100)_{\delta'}$; (*b*) CDF indicating sheared T_1, $\mathbf{b} = [110]_\alpha$, $g = \frac{1}{2}(111)_\alpha$; (*c*) HREM micrograph showing sheared T_1, $\mathbf{b} = [110]_\alpha$; and (*d*) BF image showing shear bands along $(111)_\alpha$ trace, $\mathbf{b} = [110]_\alpha$.

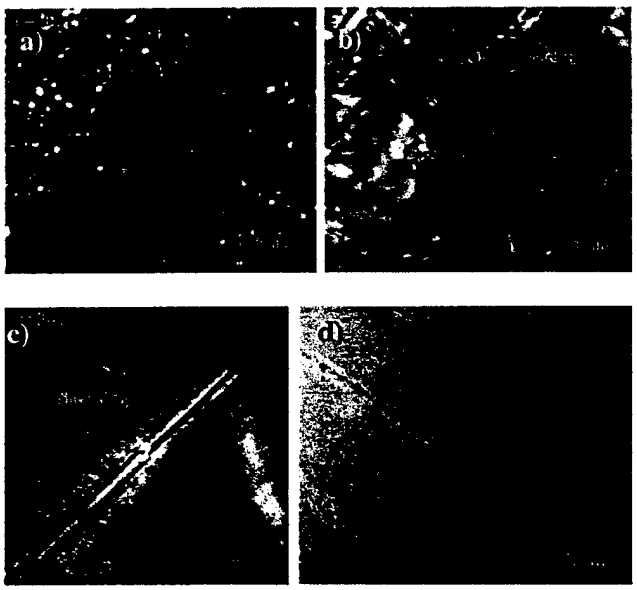

Fig. 13—AF/C-489 150 °C 24 h 2 pct plastic strained micrographs: (*a*) CDF image showing sheared δ' (arrows), $\mathbf{b} = [101]_\alpha$, $g = (100)_{\delta'}$; (*b*) WBDF indicating sheared and bowed T_1, $\mathbf{b} = [110]_\alpha$, g, $3g = \frac{1}{2}(111)_\alpha$; (*c*) HREM micrograph showing sheared T_1, $\mathbf{b} = [110]_\alpha$; (*d*) BF image showing shear bands along $(111)_\alpha$ trace, $\mathbf{b} = [110]_\alpha$.

C-489 alloy promoted the formation of the weaker θ'' at the expense of the stronger T_1 precipitate, while fine grain boundary T_1 precipitation seemed unaffected by the single and duplex ages for both AF/C-458 and AF/C-489 alloys.

Since T_1 was shown to shear, the distance between high angle grain boundaries, *i.e.*, grain size, determines the slip length for these alloy microstructures. Accordingly, the much larger grain size only exacerbates the higher δ' volume fraction for the AF/C-489 alloy, which significantly increases the number of dislocations impinging on a grain boundary as compared to the AF/C-458 alloy, as seen directly in Figures 15(a) and (b). These major differences between alloys seem to account for the much lower fracture strain of the AF/C-489 alloy when compared to the AF/C-458 alloy with similar aging.

The increased ductility of the duplex aged AF/C-489 alloy with no change in fracture mode suggests that the superposition of the smaller, weaker, and denser θ'' with the T_1 strengthening precipitates had a positive effect on the fracture process. Quantitative TEM clearly showed that the duplex aged AF/C-489 precipitated θ'' with a (001) habit plane at the expense of T_1 with a (111) habit plane, *i.e.*, θ' volume and number densities increased upward of 5- and 16-fold, respectively, as compared to the single 150 °C 24 hour age. This suggests increased ductility of the double aged AF/C-489 alloy may be due in part to the superposition of the θ'' and T_1 strengthening effects. However, more work and modeling needs to be conducted to clarify this point.

V. CONCLUSIONS

1 The precipitation response for both the AF/C-489 and AF/C-458 alloys was determined by TEM and DSC and was used to design an improved microstructure through duplex aging for AF/C-489.
2 Duplex aging of the AF/C-489 alloy resulted in significant increases in ductility by as much as 85 pct, with a small decrease of only 6.5 and 2.5 pct in yield and ultimate tensile strength, respectively. No significant improvements were found with either the duplex or triple aging practices for the AF/C-458 commercial alloy, indicating a large processing window.
3. Quantitative TEM demonstrated that the precipitation response significantly differed between the duplex aging for the AF/C-489 and AF/C-458 alloys. The duplex aged AF/C-489 alloy competitively precipitated more θ'' at the expense of T_1, whereas no significant changes in precipitation response occurred for the AF/C-458 alloy. Furthermore, shearable δ' volume fraction was calculated to be, on average, ~3 pct greater in the AF/C-489 than the AF/C458 alloy.
4. Conventional TEM also demonstrated that grain boundary T_1 precipitation was unaffected by duplex aging designed to competitively precipitate more matrix T_1 than grain boundary T_1. In fact, all investigated single and double aged samples contained grain boundary T_1.
5. Conventional TEM, HREM, and SEM fractography demonstrated that formation of shear bands occurred as a result of the localized shearing of both the δ' and T_1 strengthening precipitates in both the AF/C-458 and AF/C-489 alloys.
6. In summary, the low ductility of the AF/C-489 alloy in comparison to the AF/C458 alloy is attributed to the increased volume fraction of shearable δ' coupled with a larger grain size, both of which significantly increase the amount of strain localization and stress concentrations at grain boundaries. This results in more low energy intergranular fracture for the AF/C-489 alloy.

ACKNOWLEDGMENTS

The authors acknowledge helpful discussions with Dr. Kumar Jata during the course of this research. We also

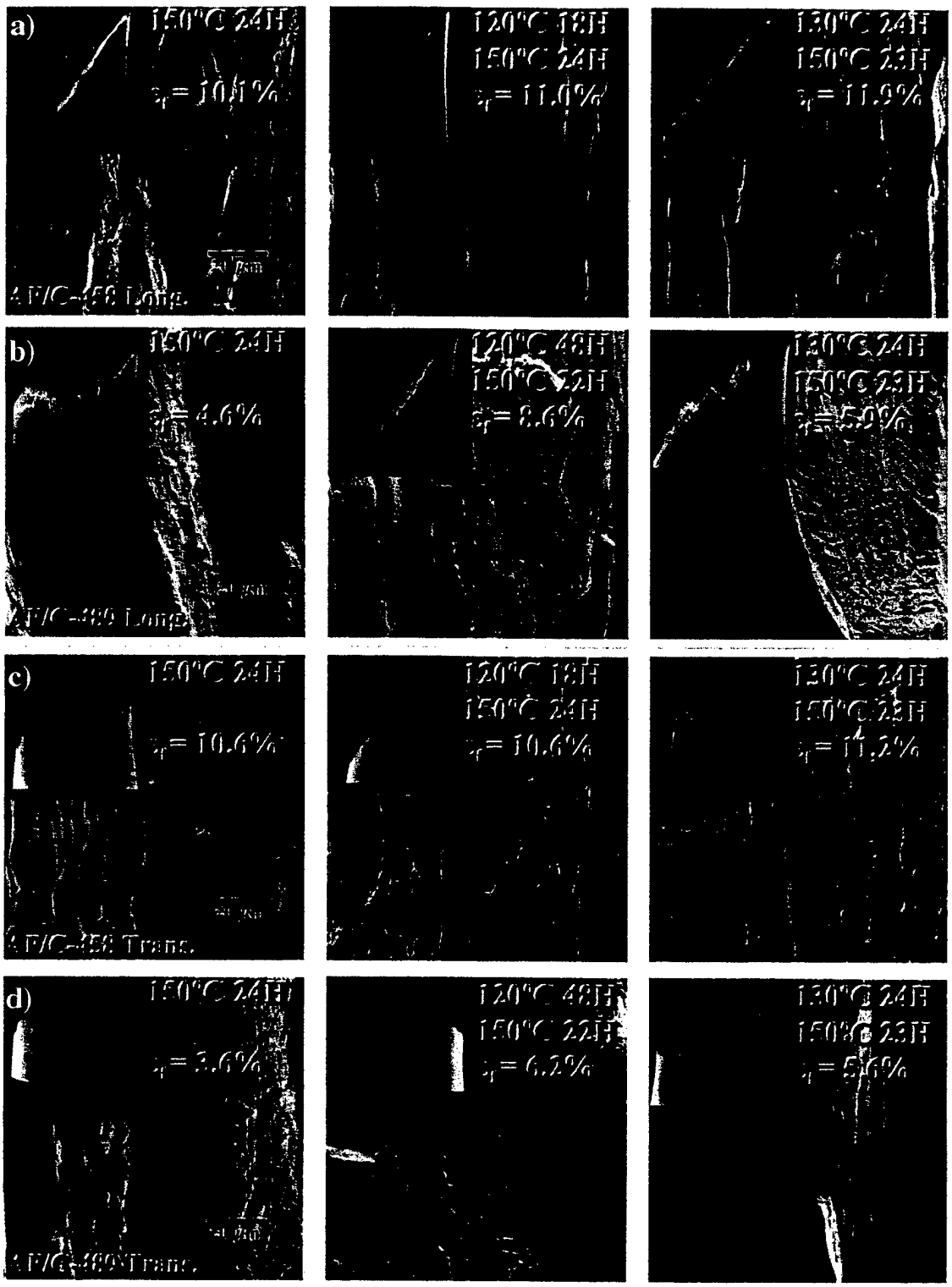

Fig. 14—(*a*) through (*d*) SEM fractography of single and duplex aged AF/C-458 and AF/C-489 alloys from longitudinal and transverse fractured tensile bars, as indicated.

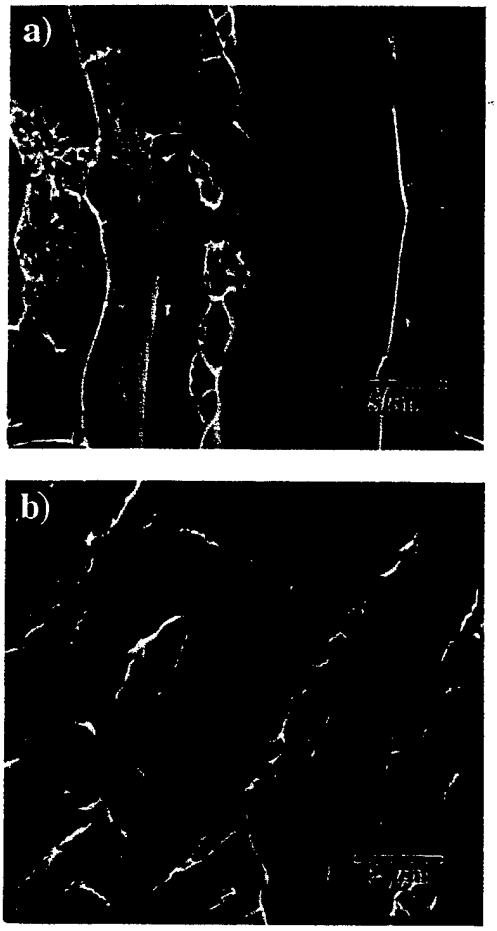

Fig. 15—SEM fractography of (*a*) longitudinal AF/C-458 aged 150 °C 24 h, indicating clean fractured grains, MVC, dimpled rupture, and no slip offsets; and (*b*) longitudinal AF/C-489 aged 150 °C 24 h, indicating slip offsets and intergranular fracture with possible grain boundary T_1 pullout.

gratefully acknowledge the support of the Air Force Office of Scientific Research under Grant No. F49620-97-1-1034, Dr. Spenser Wu, Program Monitor.

REFERENCES

1. E.A. Starke, Jr.: *Alloying*, ASM, Metals Park, OH, 1988, p. 175.
2. A.K. Vasudevan, W.G. Fricke, Jr., M.A. Przystupa, and S. Panchanadeeswaran: *ICOTOM 8*, TMS, Warrendale, PA, 1988, p. 1071.
3. C.P. Blankenship and E.A. Starke, Jr.: in *Aluminum-Lithium Alloys VI*, M. Peters and P.J. Winkler, eds., DGM Informationsgesellschaft, Oberursel, Germany, 1992, p. 187.
4. K.T.V. Rao and R.O. Ritchie: *Mater. Sci. Technol.* 1989, vol. 5, p. 882.
5. Materials Directorate, Wright Laboratory, Air Force Material Command, Wright Patterson AFB, OH, under Contract No. F33615-92-C-5914.
6. A.K. Hopkins, K.V. Jata, and R.J. Rioja: in *Aluminum Alloys, Their Physical and Mechanical Properties—Proceedings ICAA5*, J.H. Driver, B. Dubost, F. Durand, R. Fougeres, P. Guyot, P. Sainfort, and M. Suery, eds., Materials Science Forum, Vols. 217–222, Transtec Publications, Zurich, Switzerland, 1996, p. 421.
7. E.A. Starke, Jr., T.H. Sanders, Jr., and I.G. Palmer: *J. Met.*, 1981, vol. 33, p. 24.
8. D. Webster: *Metall. Trans. A*, 1987, vol. 18A, pp. 2181-93.
9. A.K. Vasudevan, A.C. Miller, and M.M. Kersker: in *Aluminum-Lithium Alloys II*, E.A. Starke, Jr. and T.H. Sanders, Jr., eds., TMS-AIME, Warrendale, PA, 1983, p. 181.
10. A.K. Vasudevan, R.D. Doherty, and S. Suresh: in *Aluminum Alloys—Contemporary Research and Applications*, 1989, vol. 31, p. 446.
11. E.A. Starke, Jr. and J.T. Staley: *Progr. Aerospace Sci.*, 1996, vol. 32, p. 131.
12. J.G. Kaufman and J.S. Santner: in *Applications of Fracture Mechanics for Selection of Metallic Structural Materials*, J.E. Campbell, W.W. Gerberich, and J.H. Underwood eds., ASM, Metals Park, OH, 1982, p. 169.
13. T.H. Sanders, Jr. and E.A. Starke, Jr.: *Acta Metall.*, 1982, vol. 30, p. 927.
14. M. Furukawa, Y. Miura, and M. Nemoto: *Trans. Jpn. Inst. Met.*, 1985, vol. 26, p. 230.
15. W.A. Cassada, G.J. Shiflet, and E.A. Starke, Jr.: *Acta Metall.*, 1986, vol. 34, p. 367.
16. G. Terlinde and G. Luetjering: *Metall. Trans. A*, 1982, vol. 13A, pp. 1283-92.
17. S. Fox, D.S. McDarmaid, and H.M. Flower: *Proc. Aluminum Technology '86*, Institue of Metals, London, 1986, Book 3.
18. A.K. Vasudevan and R.D. Doherty: *Acta Metall.*, 1987, vol. 35, p. 1193.
19. R.E. Crooks, E.A. Kenik, and E.A. Starke, Jr.: *Scripta Metall.*, 1983, vol. 17, p. 643.
20. A.K. Vasudevan and S. Suresh: *Mater. Sci. Eng.*, 1985, vol. 72, p. 37.
21. S. Suresh, A.K. Vasudevan, M. Tosten, and P.R. Howell: *Acta Metall.*, 1987, vol. 35, p. 25.
22. J.M. Duva, M.A. Daeubler, E.A. Starke, Jr., and G. Luetjering: *Acta Metall.*, 1988, vol. 36, p. 585.
23. C.P. Blankenship, Jr., E. Hornbogen, and E.A. Starke, Jr.: *Mater. Sci. Eng.*, 1993, vol. A169, p. 33.
24. M. Sugamata, C.P. Blankenship, Jr., and E.A. Starke, Jr.: *Mater. Sci. Eng.*, 1993, vol A163, p. 1
25. K.V. Jata and E.A. Starke, Jr.: *Metall. Trans. A*, 1986, vol. 17A, pp. 1011-26.
26. H.J. Roven: *Scripta Metall. Mater.*, 1992, vol. 26, p. 1383.
27. E. Hornbogen: *Z. Metallkd.*, 1975, vol. 66, p. 511.
28. T.S. Srivatsan: *J. Mater. Sci. Lett.*, 1988, vol. 7, p. 940.
29. E.A. Starke, Jr. and F.S. Lin: *Metall. Trans. A*, 1982, vol. 13A, pp. 2259-69.
30. J.A. Walsh, K.V. Jata, and E.A. Starke, Jr.: *Acta Metall.*, 1989, vol. 37, p. 2861.
31. V.K. Jain, K.V. Jata, R.J. Rioja, J.T. Morgan, and A.K. Hopkins: *J. Mater. Processing Technol.*, 1998, vol. 73, p. 108.
32. K.V. Jata, S. Panchanadeeswaran, and A.K. Vasudevan: *Mater. Sci. Eng.*, 1998, vol. A257, p. 37.
33. K.V. Jata and A.K. Vasudevan: *Mater. Sci. Eng.*, 1998, vol. A241, p. 104.
34. C.P. Blankenship and E.A. Starke, Jr.: *Metall. Trans. A*, 1993, vol. 24A, p. 833.
35. R.F. Ashton, D.S. Thompson, E.A. Starke, Jr., and F.S. Lin: in *Aluminum-Lithium Alloys III*, C. Baker, P.J. Gregson, S.J. Harris, and C.H. Peel, eds., The Institute of Metals, London, 1986, p. 66.
36. T. Ahrens and E.A. Starke, Jr.: in *Aluminum-Lithium Alloys V*, T.H. Sanders, Jr. and E.A. Starke, Jr., eds., MCE Publications Ltd., Birmingham, United Kingdom, 1989, p. 385.
37. C.P. Blankenship, Jr. and E.A. Starke, Jr.: *Scripta Metall.*, 1992, vol. 26, p. 1719.
38. C.P. Blankenship, Jr. and E.A. Starke, Jr.: *Acta Metall.*, 1994, vol. 42, p. 845.
39. W.A. Cassada, G.J. Shiflet, and E.A. Starke, Jr.: *Metall. Trans. A*, 1991, vol. 22A, pp. 287-97.
40. W.A. Cassada, G.J. Shiflet, and E.A. Starke, Jr.: *Metall. Trans. A*, 1991, vol. 22A, pp. 299-306
41. A.A. Csontos, B.M. Gable, A. Gaber, and E.A. Starke, Jr.: "The Effect of Quench Rate on the Microstructure and Properties of AF/C-458 and AF/C-489 Al-Li-Cu-X Alloys," *7th International Conference on Aluminium Alloys: Their Physical and Mechanical Properties*, Eds. E.A. Starke, Jr., T.H. Sanders, Jr., and W.A. Cassada, Trans Tech Publications, Zurich, Switzerland, pp. 1333-1340, 2000.
42. W.A. Cassada: Ph.D. Dissertation, University of Virginia, Charlottesville, VA, 1987.
43. J.E. Hilliard: *TMS-AIME*, 1962, vol. 224, p. 906.
44. D.B. Williams and C.B. Carter: *Transmission Electron Microscopy*, New York, 1996, Plenum Press, New York.

ELSEVIER

APPENDIX II

JOURNAL OF LIGHT METALS

Journal of Light Metals 1 (2001) 1–14

www.elsevier.com/locate/ligandmet

The role of plastic deformation on the competitive microstructural evolution and mechanical properties of a novel Al–Li–Cu–X alloy

B.M. Gable, A.W. Zhu, A.A. Csontos, E.A. Starke Jr. *

Department of Materials Science and Engineering, University of Virginia, 116 Engineer's Way, P.O. Box 400745, Charlottesville, VA 22904-4745, USA

Abstract

The role of plastic deformation prior to artificial aging on the microstructural evolution and mechanical properties of a novel Al–Li–Cu–X alloy designated AF/C 458 was investigated. Induced plastic deformation ranged from a non-stretched or 0% stretch condition to an 8% stretch, with intermediate stretches of 2%, 4% and 6%. Tensile properties, fractography and quantitative precipitate analysis were acquired from specimens that were water quenched from a solution heat treatment, immediately stretched and artificially aged at 150°C. Fractography was investigated through scanning electron microscopy (SEM). Quantitative transmission electron microscopy (TEM) determined the variation in precipitate type, number density, size and volume fraction of the major strengthening precipitates Al_2CuLi (T_1), Al_2Cu (θ''/θ') and Al_3Li (δ').

Age hardening curves for each level of mechanical stretch illustrated the enhanced aging kinetics of plastically deformed material. Quantitative TEM indicated that increasing amounts of pre-age stretch were found to greatly affect the competitive precipitation kinetics of T_1 and θ''/θ' in AF/C 458 augmenting the volume fraction of fine matrix T_1 plates and dramatically decreasing the volume fraction of θ''/θ' for isochronal treatments. A quantitative microstructural comparison of specimens exhibiting a given strength demonstrated that the imposed level of cold work dictated the density, size and volume fraction of the competing precipitates. The tensile data indicated a trend of increasing ductility for equivalent yield strengths with the increasing amount of pre-age mechanical stretch and therefore shorter artificial aging times. The quantitative precipitate data were used with a computer simulation for yield strength determination. The theoretical simulation reported calculated yield strengths in good accord with experimental results and can thus be used to predict the optimum microstructural configuration for high strength.

Keywords: Mechanical stretch; Competitive precipitation; Computer simulation; Aerospace materials; AF/C 458

1. Introduction and background

Plastic deformation prior to artificial aging in Al–Li–Cu–X alloys has been found to enhance the strength, ductility and aging kinetics over non-deformed material through the introduction of dislocations, which act as preferential matrix nucleation sites for the primary strengthening phase T_1 [1–15]. Increasing the amount of introduced plastic deformation leads to a greater number of matrix dislocations. An increase in the number density of nucleation sites [11] creates overlapping diffusion fields as precipitates grow, causing the average size of the precipitate to decrease. The refinement of the precipitate microstructure corresponds with the enhanced aging kinetics due to the increased number density of strengthening precipitates and the shorter time required to deplete the contiguous matrix of solute to obtain a specific strength. The increase in the volume fraction of matrix T_1 combined with the enhanced aging kinetics has been shown to lower the volume fraction of grain boundary T_1 for the peak-aged condition [3–6,8,10] and significantly lower the number density and volume fraction of θ''/θ'. Augmented T_1 volume fraction has been shown to affect Al_3Li (δ') precipitation due to limiting the available lithium for further nucleation and growth [5,6,13].

Cassada et al. [11,12] demonstrated that increasing high levels of plastic deformation prior to artificial aging for a near-2090 alloy aged at 190°C resulted in marked gains in yield strength for the under- and peak-aged conditions due to the enhanced volume fraction of fine matrix T_1. Matrix precipitation of this more abundant and finer strengthening phase directly correlates to the

* Corresponding author. Tel.: +1-804-924-6335; fax: +1-804-924-1353.

E-mail address: easlo@virginia.edu (E.A. Starke Jr.).

1471-5317/01/$ - see front matter
PII: S1471-5317(00)00002-X

increased strength and ductility of the material versus a non-stretched condition that exhibits only grain boundary T_1 precipitation [4–6,13]. Recent computer models by Zhu et al. [16] suggest that the strengthening effect of matrix precipitation is optimized through the presence of two unshearable plate precipitates with {1 1 1} and {1 0 0} habit planes, i.e., T_1 and θ''/θ', respectively.

Although it has been known for many years that a stretch prior to aging introduces dislocations that subsequently act as nucleation sites for precipitates with large interfacial strains, no systematic study has been conducted on the effect of stretch when different types of precipitates are in competition for preferential matrix nucleation sites and solute atoms.

This study investigated the role of varying prior plastic deformations on the competitive precipitation kinetics of the primary strengthening phases Al_2CuLi (T_1) and Al_2Cu (θ''/θ'). Quantified transmission electron microscopy (TEM) data were related to the subsequent tensile properties of AF/C 458, namely strength and ductility. Number density, size and volume fraction comparisons of the $T_1, \theta''/\theta'$ and δ' strengthening precipitates were performed in order to quantify the competitive precipitation kinetics as a function of thermomechanical processing for the alloy. These quantitative data were then used as a means of challenging the validity of recent computer simulations [16].

2. Experimental procedure

Alcoa fabricated the Al–2.7Cu–1.8Li–0.6Zn–0.3Mg–0.3Mn–0.08Zr (w/o) alloy designated AF/C 458 used in this study. The alloy was ingot cast, homogenized and subsequently formed through a two-stage rolling process. The unrecrystallized plate underwent a 6% tensile stretch in the longitudinal direction resulting in a 1.905×10^{-2} m through-thickness plate. This is considered the "as-received" material.

Tensile samples were machined in accordance with ASTM E8- 93 [17] parallel to the rolling direction of the as-received plate. These specimens were then solution heat treated in a Lindberg three-zone furnace at 540°C for 1 h and subsequently water quenched (290°C/s) and immediately stretched. The pre-age stretch was performed immediately upon quenching [13] from the solution heat treatment to minimize the effects of an inhomogeneous dislocation structure arising from the presence of shearable naturally aged δ' precipitates [18]. The tensile specimens were stretched on an MTS Sintech 10/GL frame employing a crosshead displacement of 1×10^{-4} m/min. The real-time elongation of each specimen was observed through a digital display via a computer interface with a MTS extensometer across an initial gauge of 0.025 m. The extent of imposed plastic deformation ranged from a non-stretched or 0% stretch condition to an 8% stretch, with intermediate stretches of 2%, 4% and 6%. The tensile samples were aged in a Stabil–Therm box furnace at 150°C for various times to investigate the mechanical properties and microstructural evolution of the alloy as a function of prior plastic deformation. The reported tensile data are an average of at least duplex specimens.

Age hardening curves based upon the obtained tensile data for each stretch condition were obtained. Each tensile specimen was subjected to tensile loading until fracture on the same MTS Sintech 10/GL frame at a crosshead displacement of 0.003 m/min to obtain strength and ductility data. An isochronal investigation was conducted to quantify the role of stretch on competitive matrix precipitation. The age hardening curves allowed for the comparison of the microstructural evolution of specimens of a given yield strength but varying levels of plastic deformation and artificial aging time.

Representative fractography specimens were sectioned from fractured tensile samples and mounted for scanning electron microscopy (SEM) investigation. A Zeiss DSM field emission gun (FEG) SEM was used for the fractographic investigation. Specimens were sectioned from untested tensile specimens for TEM investigation on a JEOL 2000FX. Once sectioned, the specimens were ground to approximately 150 μm, punched to into 3 mm disks, and chemically thinned using a 7:2 methanol–nitric solution cooled to −24°C in a Struers Tenupol-3 electropolishing unit that produced electron transparent foils for TEM observation.

Through traditional point counting methods the number density, size and volume fraction of the primary strengthening precipitates were quantified from the transmission electron micrographs taken near $\mathbf{B} = [1\,1\,0]$. Quantitative analysis required the foil thickness of each captured region, which was obtained through convergent beam electron diffraction (CBED) patterns [19,20], and a stereological method of correction based upon the size of the precipitates relative to the thickness of the TEM foil [21,22].

The quantified precipitate data for each thermo-mechanical condition were then implemented in a computer simulation that calculated the theoretical yield strength. The precipitate type, volume fraction and dimensions were required for simulation, which accounted for disk-like precipitation on {1 1 1} and {1 0 0} habit planes, T_1 and θ''/θ', respectively, and homogeneous shearable point-like particles, δ'. The simulation was based upon the stress required to pass a dislocation through a matrix consisting of the complex four-phase microstructure. Additional terms encompassing the matrix and solid solution strengthening effects were also taken into account.

3. Results

3.1. Artificial aging characteristics

Age hardening curves in terms of yield strength were determined for each level of mechanical stretch, as shown in Fig. 1. This plot illustrates the enhanced aging kinetics and yield strength with greater amounts of pre-age stretch.

The first aspect of this study was to examine the aging characteristics of AF/C 458 as a function of the imposed level of mechanical stretch prior to artificial aging for an isochronal treatment. The second aspect of this study was to investigate the microstructural evolution of material that experienced varying thermo-mechanical processings, namely different levels of pre-age stretch and artificial aging times, to obtain similar yield strengths.

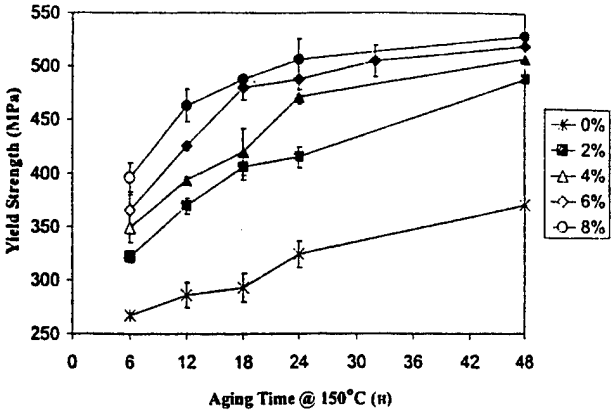

Fig. 1. Age hardening curve for various levels of pre-age stretch artificially aged at 150°C.

3.1.1. Tensile data – 150°C for 24 h

The tensile data from the specimens that were aged at 150°C for 24 h are given in Table 1. There is a marked trend of increasing strength with pre-age stretch. It is important to note the marked gains in strength between the 0% and 2% stretch conditions. There were continued gains with increasing levels of stretch, but to a lesser extent. The increased strength for each successive stretch condition was not accompanied by concomitant losses in ductility. The strength × ductility factor increased with increasing levels of stretch, resulting in over a 25% improvement between the extreme pre-age stretch conditions. For brevity the 0%, 4% and 8% specimens were used for the remaining fractographic and microstructural comparisons for the isochronal treatment.

3.1.2. Tensile data – isostrength specimens

The yield strength of 450 MPa was chosen as the basis for comparison between the various stretch conditions. Material in the under-aged condition was desirable to avoid possible difficulties with quantifying an over-aged structure. The comparison of the tensile data and artificial aging times for the five stretched conditions may be seen in Table 2. Note that a direct relationship exists between the level of imposed pre-age mechanical stretch and the required artificial aging time, with the most dramatic difference again being between the non-stretched and 2% stretch specimens. Furthermore, note that a possible trend of increasing ductility with the amount of mechanical stretch between heat treatments occurred.

Table 1
Tensile data after 150°C for 24 h

Quench media (cooling rate)	Pre-age stretch (%)	Yield strength (MPa)	S.D.	Tensile strength (MPa)	S.D.	Elongation (%)	S.D.
Water quench (290°C/s)	0	324	12.6	434	12.8	12.9	1.2
	2	415	9.8	473	15.3	10.3	0.9
	4	471	7.0	513	1.5	10.4	0.6
	6	488	15.5	519	12.8	9.9	0.6
	8	506	19.6	531	21.1	10.6	1.5

Table 2
Tensile data for T8x specimens with similar strengths

Quench media (cooling rate)	Pre-age stretch (%)	Aging time (h)	Yield strength (MPa)	Tensile strength (MPa)	Elongation (%)
Water quench (290°C/s)	0	120	454	515	9.1
	2	35	452	503	9.1
	4	20	451	500	9.9
	6	15	452	496	10.9
	8	10	452	497	10.5

3.2. Scanning electron microscopy

3.2.1. Fractography for 24 h at 150°C

The micrographs in Fig. 2 indicate predominant 45° slant fracture for each tensile specimen. Each of the fracture surfaces has regions of transgranular fracture, dimple rupture and grain boundary delamination. It is important to note that each of these conditions should have approximately the same amount of grain boundary precipitation. For the isochronal aging treatment the higher the imposed level of deformation prior to aging, the stronger the specimen although the strain to fracture was approximately the same. The latter result is most likely related to similar grain boundary precipitation.

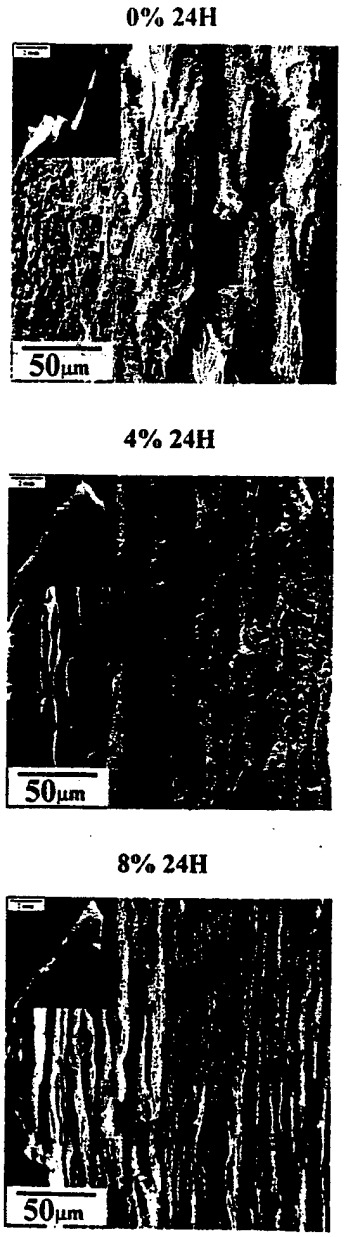

Fig. 2. SEM fractography of specimens aged for 24 h at 150°C; the low-magnification composites illustrate the macroscopic fracture angle of a tensile sample and a representative region of the fracture surface.

3.2.2. Fractography for 450 MPa specimens

The fractography of the isostrength specimens may be found in Fig. 3. Each tensile specimen exhibits 45° slant fracture with some degree of transgranular fracture and grain boundary delamination. There appears to be a trend of increasing transgranular fracture with increasing levels of stretch, which may be related to decreasing artificial aging times and subsequent grain boundary T_1 growth. Those specimens aged at longer times appear to have more intergranular failure coupled with grain boundary delamination, which correlates with more pronounced grain boundary precipitation.

3.3. Transmission electron microscopy

As stated previously, the 0%, 4% and 8% stretch conditions were utilized for quantitative microstructural comparison. Matrix precipitation of T_1, θ''/θ' and δ' strengthening phases were quantitatively measured.

3.3.1. Microstructure for 24 h at 150°C

The TEM micrographs in Fig. 4 illustrate the θ''/θ' and T_1 matrix precipitation as a function of the mechanical stretch. The most significant microstructural change is evident between the unstretched and stretched conditions. The precipitation of the 0% stretch samples is predominantly comprised of grain boundary T_1 along with matrix θ''/θ' and δ', with the occasional matrix T_1 plate that precipitated on residual matrix dislocations. It is important to note the θ''/θ' precipitate-free zone that is contiguous to the grain boundary T_1. Both the 4% and 8% stretch conditions indicate significant matrix T_1 precipitation relative to the unstretched specimen.

3.3.2. Microstructure for 450 MPa specimens

Figs. 5 and 6 illustrate the respective matrix precipitation for those specimens with yield strengths of approximately 450 MPa. The centered dark field images highlighting δ' precipitation, Fig. 5, make it possible to visualize the relative number density and size of the matrix θ' due to the wetted exterior. There appears to be a trend of decreasing θ' diameter with increasing pre-age stretch. Similarly, in Fig. 6, the shorter aging times appear to correlate with a finer T_1 plate structure.

3.4. Quantitative microstructural analysis

Optical point counting and stereological correction methods were utilized to obtain the number density, size and volume fraction of the primary strengthening phases T_1, θ''/θ' and δ' for each condition. The stereological correction method is necessary to account for particle truncation when the precipitates are large rela-

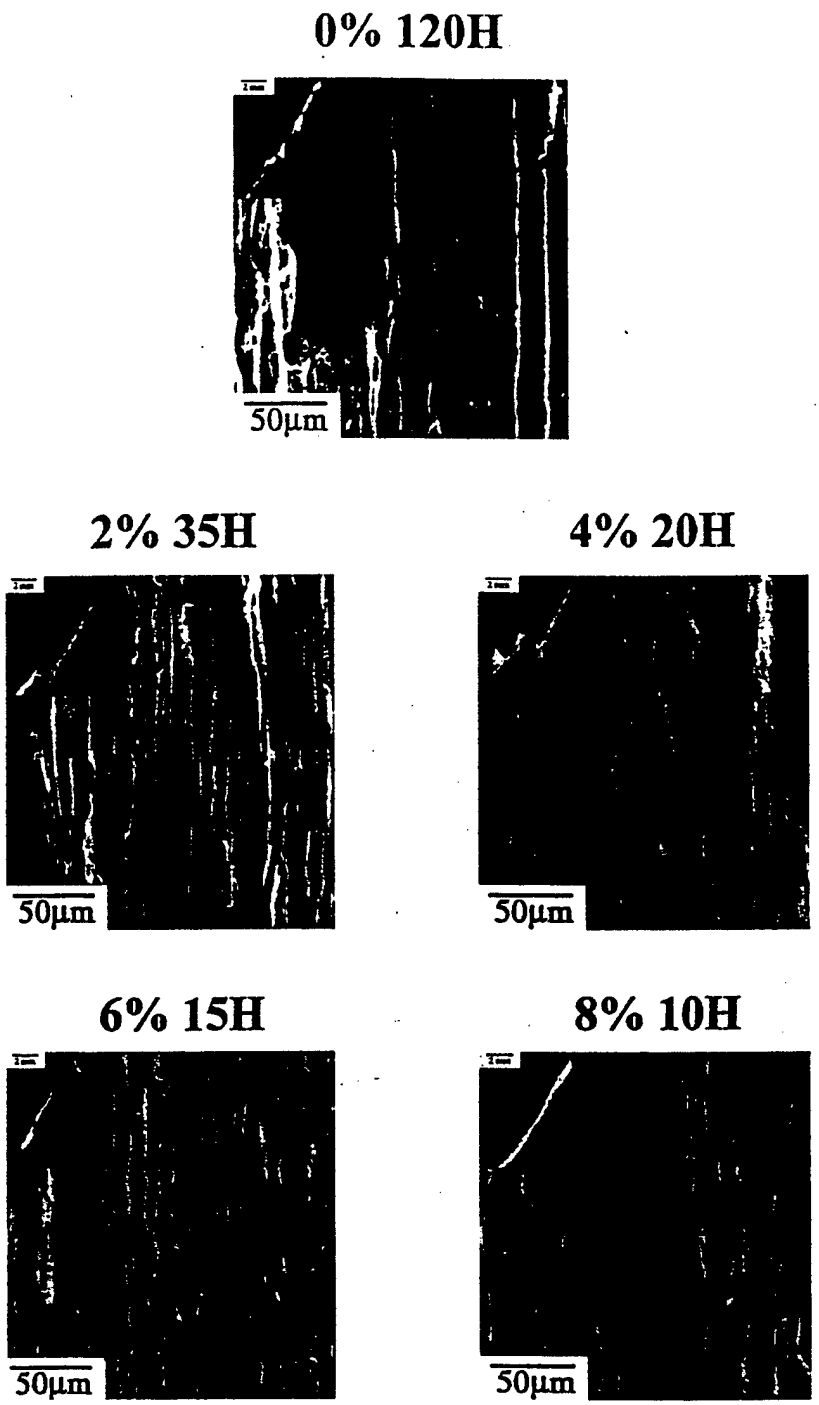

Fig. 3. SEM fractography specimens stretched different percentages and aged for various times at 150°C to obtain a yield strength of 450 MPa.

tive to the thickness of the examined foil [12]. The 0%, 4% and 8% stretch specimens were used for microstructural comparison, as in the fractography study.

3.4.1. Strengthening precipitate data for 24 h at 150°C

Table 3 conveys the quantified number density, diameter and volume fraction data for T_1, θ''/θ' and δ' as a function of prior deformation that was aged for 24 h at 150°C. Table 3 indicates that θ''/θ' dominates the matrix precipitation in the unstretched condition relative to T_1. Conversely, the imposed deformation prior to aging dramatically increased the number density and volume fraction of matrix T_1, which continued with increasing levels of deformation. These quantified microstructural data demonstrate that the enhanced precipitation of matrix T_1 dominates that of θ''/θ' for a pre-age stretched condition. Table 3 also illustrates a non-linear trend for the corrected plate diameter for both T_1 and θ' as a

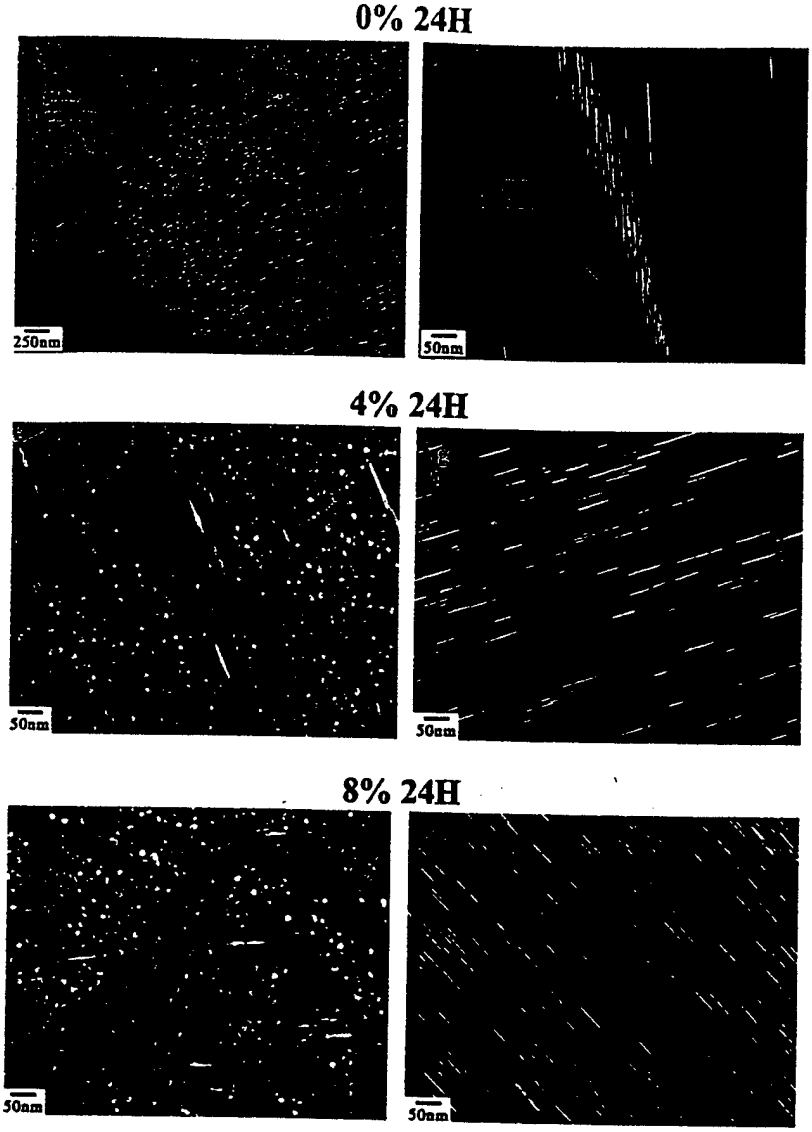

Fig. 4. TEM micrographs illustrating the matrix precipitation of specimens after aging at 150°C for 24 h. Each condition has a centered dark field image conveying matrix θ''/θ' and δ', $g = 1/2(2\,0\,0)$; and a centered dark field image for matrix T_1 precipitation, $g = 1/2(\bar{1}\,\bar{1}\,1)$. Note the affect of the grain boundary on θ'' precipitation in the 0% stretch condition.

function of pre-age stretch, which will be discussed hereafter. It is important to note that the thickness of the plates was not found to change for any artificial aging or stretch condition. The measured thickness of the T_1 plates was found to be on average 1.2 nm. The only difference in thickness was between the θ'' (0.8 nm) and θ' (1.2 nm) from the unstretched condition.

There is an apparent trend of decreasing volume fraction of δ' with increasing levels of stretch. This relationship would be expected due to the enhancement of T_1 precipitation, however, it is important to note the significant error associated with the calculated values. There does not appear to be a trend between the measured δ' diameter and the imposed level of predeformation.

3.4.2. Strengthening precipitate data for 450 MPa specimens

Table 4 indicates the quantified number density, diameter and volume fraction data of T_1, θ''/θ' and δ' for the various stretched and aged specimens that exhibited yield strengths of approximately 450 MPa.

The quantified number densities for the precipitates were found to increase with the level of imposed mechanical stretch as illustrated in Figs. 5 and 6. Conversely, there is an apparent trend of decreasing precipitate diameter and volume fraction with increasing level of pre-age stretch for each precipitate. This relationship will be developed further, specifically considering the role of the stereological correction method on plates of very different sizes. As for the isochronal heat

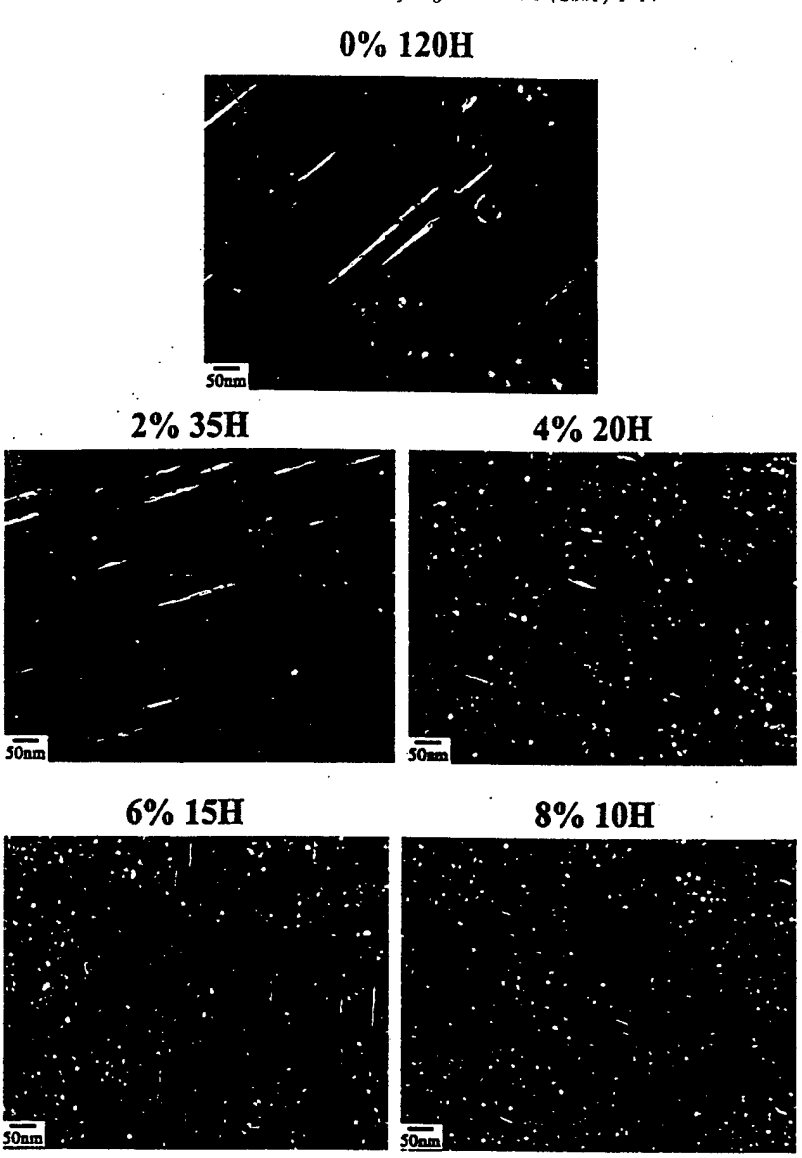

Fig. 5. TEM centered dark field micrographs illustrating δ' and wetted θ' matrix precipitation of the specimens that experienced various levels of pre-age stretch and were aged to obtain yield strength of 450 MPa. For each condition $g = 1/2(2\,0\,0)$.

treatment the thickness of the plates was determined to remain constant.

The results from the theoretical simulation on the quantitative data for the isochronal and isostrength conditions may be found in Tables 5 and 6, respectively. There are dramatic similarities between the experimental and calculated yield strengths for the isochronal specimens. The theoretical values for each stretch condition are within several percent of those obtained through laboratory tensile testing. Similarly, the calculated yield strengths for the isostrength specimens were quite good. There is a noticeable decreasing trend between the level of imposed stretch and the simulated yield strengths. This phenomenon will be discussed later.

4. Discussion

4.1. The role of mechanical stretch

4.1.1. Specimens aged for 24 h at 150°C

Initially, the relationship between the role of stretch and the microstructural evolution of AF/C 458 was investigated by obtaining tensile data for specimens that had undergone 0%, 2%, 4%, 6% and 8% mechanical stretches prior to artificial aging at 150°C for 24 h. These specimens conveyed a direct trend of increasing aging kinetics and strength with increasing levels of pre-age stretch. It is important to note that there was greater than a 50% gain in yield strength for the isochronal condition between the non-stretch and 8% stretch specimens, with a

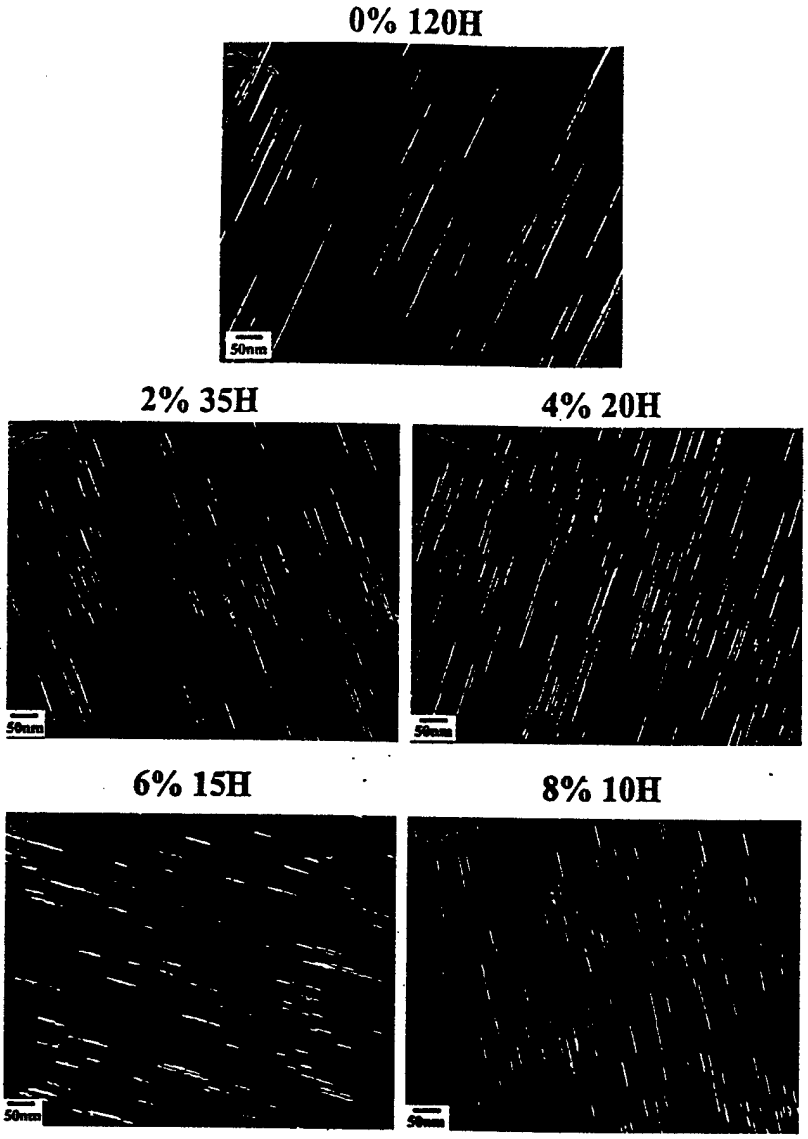

Fig. 6. TEM centered dark field micrographs illustrating matrix T_1 precipitation of specimens that experienced various levels of pre-age stretch a were aged to obtain yield strength of 450 MPa. For each condition $g = 1/2(\bar{1}\ \bar{1}\ 1)$.

Table 3
Quantitative precipitate data after 150°C for 24 h

Quantitative analysis	Stretch (%)	T_1 (Al_2CuLi)	S.D.	θ''/θ' (Al_2Cu)	S.D.	δ' (Al_3Cu)	S.D.
Number density (#/μm³)	0	286.0	50.0	6277.0	1023.0	15030.0	5677.5
	4	916.2	280.2	493.8	382.8	15691.6	865.8
	8	3035.0	183.9	176.4	106.0	12585.4	628.5
Precipitate diameter (nm)	0	64.7	2.2	33.9	0.9	12.1	2.0
	4	80.1	5.0	63.2	8.4	11.8	1.7
	8	49.8	4.6	38.4	3.9	12.2	1.9
Volume fraction (%)	0	0.52	0.17	1.14	0.14	11.10	2.25
	4	2.23	0.23	0.54	0.27	10.70	1.63
	8	2.84	1.00	0.07	0.04	9.50	1.50

minor loss in ductility. There was only a slight decreasing trend between elongation and the level of stretch, indicating the positive effect that the stretch has on the strength × ductility factor. The subsequent quantitati microstructural analysis of various stretched conditior demonstrated a direct trend between the imposed level

Table 4
Quantitative precipitate data for specimens with a yield strength of 450 MPa

Quantitative analysis	Pre-age stretch (%)	Aging time (h)	T_1 (Al_2CuLi)	S.D.	θ' (Al_2Cu)	S.D.	δ' (Al_3Li)	S.D.
Number density (#/μm³)	0	120	272.6	73.0	359.4	96.9	7778.0	1490.3
	2	35	754.7	250.2	387.9	139.8	11356.5	1276.9
	4	20	963.1	69.4	512.4	115.6	17359.6	2798.9
	6	15	1283.1	337.7	548.6	180.1	22885.4	6332.6
	8	10	1478.3	582.9	835.7	434.4	23675.4	11117.4
Precipitate diameter (nm)	0	120	158.7	12.5	88.2	30.3	16.3	3.7
	2	35	86.8	8.8	81.3	9.0	13.2	2.2
	4	20	55.6	6.0	40.1	3.6	11.9	2.0
	6	15	53.6	7.7	42.8	7.1	10.7	1.8
	8	10	40.1	5.7	28.5	5.0	10.6	1.6
Volume fraction (%)	0	120	2.53	0.47	0.95	0.73	14.00	5.00
	2	35	2.12	0.51	0.65	0.39	10.90	2.19
	4	20	1.64	0.82	0.23	0.05	12.30	3.21
	6	15	1.42	0.37	0.30	0.09	11.70	5.25
	8	10	0.94	0.58	0.20	0.15	11.70	8.27

Table 5
Computer simulation results for isochronal condition

Pre-age stretch (%)	Aging time (h)	Measured yield strength (MPa)	Calculated yield strength (MPa)	Deviation (%)
0	24	324	302	−6.8
4	24	471	490	4.0
8	24	506	488	−3.6

Table 6
Computer simulation results for isostrength specimens

Pre-age stretch (%)	Aging time (h)	Measured yield strength (MPa)	Calculated yield strength	Deviation (%)
0	120	454	494	8.8
2	35	452	479	6.0
4	20	451	420	−6.9
6	15	452	438	−3.1
8	10	452	396	−12.4

plastic deformation, yield strength and the number density and volume fraction of matrix T_1 precipitates. Conversely, the pre-age stretch dramatically lowered the number density and volume fraction of θ''/θ'. This may indicate the predominance of T_1 in the competition for heterogeneous matrix nucleation sites. This illustrates a direct correlation between the imposed level of stretch, i.e., the matrix dislocation density, and the number of quantified T_1 and θ''/θ' precipitation events.

The obtained tensile data for the various pre-age stretched conditions, found in Table 1, indicate an initial "jump" of 28% (91 MPa) in yield strength associated with a 2% stretch. This relationship is directly related to the augmented matrix precipitation of T_1 relative to that of θ''. It is important to remember that the dense population of θ'' in the unstretched condition is adversely affected through the addition of matrix dislocations. These findings are in good agreement with the earlier studies that focused on the number density and precipitate diameter of competing phases in Al–Cu–X systems [11–14].

The enhanced aging kinetics of a given stretch condition directly correlates with the marked increase in the number density of matrix T_1. The increase in the number density of nucleation sites decreases the average distance between precipitates. This interparticle spacing is the limiting factor in the soft impingement of neighboring precipitates. The greater the number of nucleation sites, the finer the distribution of plates, the smaller the average diffusion field, and therefore the shorter the time required to deplete the surrounding matrix. The enhanced aging kinetics of increasing levels of plastic deformation was illustrated in the age hardening curves seen in Fig. 1 and the time required for specimens to obtain a yield strength of 450 MPa in Table 2.

In a similar fashion, there is a direct correlation between the quantified number density of T_1 and θ''/θ' and the respective measured volume fraction, as shown in Table 3. The matrix precipitation for the unstretched condition is dominated by θ'', due to the few residual dislocations allowing for preferential T_1 and θ' nucleation. Furthermore, increasing the level of pre-age stretch dramatically increased the number of heterogeneous matrix nucleation sites, which affected the competitive precipitation kinetics between T_1 and θ''/θ', resulting in a marked shift in the relative volume fraction.

The quantified precipitate diameters also lend themselves to discussion. The data in Table 3 do not convey

any apparent linear trends between the size of either T_1 or θ''/θ' as a function of imposed mechanical stretch. However, the quantified relationships may be explained. For both precipitates there was a measured increase in precipitate size between the 0% and 4% stretch conditions followed by a refinement with increasing stretch to 8%. The increase in average size for the θ''/θ' between the 0% and 4% stretch conditions is due to the introduction of heterogeneous matrix nucleation sites. Although not supported through high-resolution microscopy, it is believed that the matrix precipitation in the unstretched condition is comprised solely of θ'' for early artificial aging times, rather than θ'. This is taken from the literature [1,23–25] in which case θ'' is the preferred matrix precipitate when there is an insufficient number of matrix heterogeneous nucleation sites. This increase in quantified diameter correlates with the transition from θ'' to θ' with the significant loss in number density due to the presence of both θ' and T_1. The refinement of both θ' and T_1 with stretch to increasing 8% was due to an increase in the number density of nucleation sites which directly relates to overlapping diffusion fields, leading to finer precipitates.

It is important to recall the early work of Silcock [1] that investigated the role of introducing heterogeneous matrix nucleation sites, in the form of cadmium additions and matrix dislocations through a pre-age stretch. Focusing on the mechanical stretch aspect, the author found that for cold worked material the precipitate that preferentially nucleated and grew in an Al–Li–Cu ternary was dictated by the alloy's chemistry. In a high copper containing alloy the dominant precipitate that preferentially nucleated and grew was θ'. An alloy with an additional 0.5 wt%Li exhibited an increase in the intensity of T_1 diffraction spots relative to those of θ'. Similarly, T_1 was more dominant with respect to θ' in a lithium-rich alloy. This indicates that the driving force for the preferential precipitation is a function of the relative saturation of the matrix, or the Li:Cu ratio. This ratio may indicate a significant driving force for the precipitation of either T_1 or θ', given heterogeneous matrix sites.

Several pertinent studies on Al–Li–Cu–X alloys have been summarized in terms of their Li:Cu ratios in Table 7. All of these ratios were calculated assuming a constant lithium solubility of 2.0 at.% and negligible copper solubility. In the case of AF/C 458, the copper content was adjusted due to the presence of manganese (AF/C 458 utilizes two types of dispersoids, one of which is an $Al_{20}Mn_3Cu_2$ type). The ratios reported are in terms of super-saturated atoms, i.e., those atoms available to form secondary phases. It is important to note that the Li:Cu atomic ratio for AF/C 458 is approximately 9:2. Note that the ratio for the copper-rich alloy from the Silcock study, in which θ' dominated, was less than 1.0 whereas the remaining alloys exhibited dominance by T_1 and had a Li:Cu greater than 1.0. Stoichiometrically, the Li:Cu ratio must be greater than 1.0 for T_1 (Al_2LiCu) to possibly control the competitive co-precipitation with θ' (Al_2Cu).

A study by Noble and Thompson [2] investigated two Al–Li–Cu alloys, one copper-rich with moderate lithium (alloy A), and the other with low copper and higher lithium (alloy B). These alloys are also included in Table 7. The investigators found that alloy A, the copper-rich alloy with moderate lithium, had homogeneous grain boundary and matrix precipitation of T_1 *without* the addition of matrix heterogeneous sites. This indicates that the relative super-saturation of the matrix overcame the barrier for homogeneous matrix nucleation. Conversely, the copper-poor alloy, alloy B, only exhibited matrix T_1 precipitation along grain boundaries and matrix dislocations. Due to the decrease in chemical driving force, from the less-saturated matrix, T_1 precipitation required further reduction of the interfacial and strain energy barriers for nucleation in the form of matrix dislocations. Noble and Thompson noted that the change in precipitation indicated a loss in the driving force for T_1 precipitation.

The kinetics of co-precipitation are based upon the combinations between lattice defects, i.e., heterogeneous nucleation sites, that minimize the energy barrier for nucleation and the rate of formation for the competing phases [24]. The phases in competition with one another

Table 7
Atomic Li:Cu ratios for various Al–Li–Cu–X alloys of interest

Investigation [reference]	Alloy	Lithium (wt%)	Copper (wt%)	Predominant phase in T8x		Li:Cu ratio (atomic)
				θ'	T_1	
Current study	AF/C 458	1.80	2.70		X	4.43
Noble & Thompson [2]	Alloy A	3.50	3.50		X	2.19
	Alloy B	1.50	2.50		X	4.90
Silcock [1]	#1	1.00	3.50	Very strong	Weak	0.88
	#2	1.50	3.50	Medium	Medium	2.19
	#3	2.00	1.00	Very weak	Weak	12.24
Cassada [11,12]	Near-2090	2.45	2.45		X	6.68

then form simultaneously at their respective preferred sites. The less stable phase dissolves sacrificially during growth, with the more stable phase becoming more predominant, ruling the competitive precipitation. When in competition the dominant precipitate is the one with the lowest energy barrier for a given lattice defect. The energy barrier for a given site in a certain alloy is dependent upon the misfit strain energy, interfacial energy, and the driving force associated with local supersaturation, for example.

Additional driving force for the preferential nucleation of T_1 and θ' near a matrix dislocation comes from the reduction of the energy barrier for that particular precipitate. In the case of Al_2Cu, θ'' is the preferred matrix precipitate when heterogeneous sites are absent because of the high coherency between θ'' and the matrix. Despite the lowest relative driving force due to thermodynamic stability, θ'' nucleates due to the minimal interfacial energy barrier [23]. Once heterogeneous nucleation sites with sufficient strain fields, e.g., dislocations, are introduced into the matrix the associated strain lowers the misfit for the thermodynamically more stable phase, θ', allowing it to preferentially nucleate and grow [23,24]. This explains the shift from θ'' to θ' between the unstretched and stretched conditions, respectively.

Cahn [25] has derived equations for the rates of heterogeneous nucleation at various defects in a solid. For nucleation on dislocations, Cahn assumed elastic and surface isotropy and an incoherent nucleus and expresses his results in terms of a dimensionless parameter [26]

$$\alpha = \Delta G_v \mu b^2 / 2\pi^2 \sigma^2, \quad (1)$$

where ΔG_v is the change in volume-free energy, μ the shear modulus, b the Burgers vector and σ is the interfacial energy required to form a new surface. The effectiveness of a dislocation in catalyzing nucleation increases as α increases and thus as ΔG_v and the magnitude of the Burgers vector increases as the surface energy decreases.

The change in volume-free energy associated with the precipitation of T_1 may be larger than that associated with θ' since T_1 is an equilibrium phase and θ' is a metastable phase. Calculated interfacial energies for the δ', θ'', θ' and T_1 precipitates may be found in Table 8. These data illustrate the relative energy barriers for the competing phases for various precipitate–defect combinations. It is important to recall that fundamental data, such as interfacial energies, are a strong function of various metallurgical factors, e.g., alloy composition, and should only be taken as relative values. Nicholson [32] has pointed out that although the present theory of heterogeneous nucleation is qualitatively satisfactory, it cannot be applied in a quantitative form in real systems because of the lack of accurate interfacial energy data relating to a defect and a nucleus. However, if we assume that the values in Table 6 are correct relative to one another we can discuss the competitive precipitation kinetics for this alloy, which is in strong agreement with the quantified data from this investigation. As in Table 3, θ'' nucleation dominates the matrix for short times in the absence of heterogeneous sites, namely dislocations. In the presence of defects that lower the energy barrier for nucleation, both θ' and T_1 plates nucleate and grow due to the enhanced thermodynamic driving force.

Although the interfacial energies of θ' and T_1 are similar, their corresponding volumetric strains differ by an order of magnitude. In addition, their shear strains, although very similar, lie on different planes and along different directions, Table 9 [33,34]. The shear strain associated with θ' has a magnitude of 0.333 on the $(0\,0\,1)_\alpha$ plane in the $[1\,0\,0]_\alpha$ direction, while the shear strain associated with T_1 has a magnitude of 0.354 on the $(1\,1\,1)_\alpha$ plane in the $[1\,1\,\bar{2}]_\alpha$ direction [33,34]. Since the volume strain energy is substantially smaller than the shear strain energy, the manner in which the shear component of the strain associated with the formation of the precipitate is accommodated may be the key factor in controlling nucleation behavior [33]. Since the shear strain for T_1 is in the plane of the Burgers vector of dislocations in the aluminum matrix, i.e., {1 1 1} planes, dislocations may thus have a greater effect on its nucleation than that of θ'. It thus appears that a combination of the larger ΔG_v and the {1 1 1} shear strain for T_1 aids in its preferential nucleation on dislocations over that of θ' given an appropriate alloy composition. This is supported by our quantified data that the relative

Table 8
Calculated interfacial energies for precipitates

Type of precipitation [reference]	δ' (Al_3Li)	Interfacial energy (J/m^2)			T_1 (Al_2LiCu)
		GP_1 zone	θ'' (Al_2Cu)	θ' (Al_2Cu)	
In the presence of dislocations [27]	–	–	–	–	0.13–0.23
Matrix precipitation [28]	–	0.003	–	–	–
Matrix precipitation [29]	–	–	0.05	–	–
Matrix precipitation [30]	–	–	–	0.179	–
Matrix precipitation [31]	0.014	–	–	–	–

Table 9
Precipitate structural data [33,34]

Phases	θ' (Al_2Cu)	T_1 (Al_2CuLi)
Crystal structure	Tetragonal	Hexagonal
Lattice parameter	$a = 0.404$ nm	$a = 0.496$ nm
	$c = 0.580$ nm	$c = 0.935$ nm
Orientation	$(0\,0\,1)_{\theta'}//(0\,0\,1)_{\alpha}$	$(0\,0\,0\,1)_{T_1}//(1\,1\,1)_{\alpha}$
Relationship	$[0\,0\,1]_{\theta'}//[1\,0\,0]_{\alpha}$	$[1\,0\,\bar{1}\,0]_{T_1}//(1\,\bar{1}\,0)_{\alpha}$
Habit plane	$\{1\,0\,0\}_{\alpha}$	$\{1\,1\,1\}_{\alpha}$
Volumetric strain	−0.05698	−0.00723
Shear strain	0.33333	0.35355
E_S/E_V	40	10 000

driving force for T_1 nucleation and growth is greater than that for θ' in AF/C 458 when matrix dislocations are present.

4.1.2. Isostrength specimens

The second aspect of this investigation was to compare the microstructural evolution for specimens with similar yield strengths as a function of the thermo-mechanical processing, namely the imposed pre-age mechanical stretch and the artificial aging time.

The tensile data in Table 2 convey a trend of increasing ductility for equivalent yield strength with the increasing amount of pre-age mechanical stretch and therefore shorter artificial aging times. This structure–property relationship should be directly related to the aspects of the grain boundary precipitation, namely the average dimension, volume fraction and grain boundary area covered. Each of these aspects is a function of the artificial aging time. With the longer the artificial aging time, the greater the grain boundary precipitation and the lower the ductility of the specimen. Nevertheless, note that each specimen exhibited at least 9% elongation even after artificial aging for 120 h, which is nearly twice the acceptable value for aerospace applications [18].

As shown in Table 4, the quantified precipitate microstructure of the various conditions illustrates three linear trends with the increasing mechanical stretch. First, the number densities of both T_1 and θ' were found to increase with the level of pre-age stretch, which relates to the enhanced matrix dislocation density and aging kinetics. The number density of δ' was also found to increase with the level of imposed stretch. The dislocation density directly relates to the number of precipitation events and, therefore, required aging time to achieve a given strength. The fewer the matrix dislocations the longer the required aging time and the coarser the microstructure.

Similarly, the corrected plate diameter for each precipitate was found to decrease with increasing pre-age stretch as illustrated in Figs. 5 and 6. This illustrates that the plate length, or sphere diameter in the case of δ', is a direct function of the artificial aging time with a very fine microstructure resulting from high levels of mechanical stretch. Conversely, the coarse precipitate structure of large T_1 and θ' plates and δ' spheres is due to prolonged exposure at artificial temperatures for those specimens experiencing a lower amount of plastic deformation prior to aging.

The quantitative precipitate data suggest that a large number of fine matrix plates and spheres, as in the high-stretch conditions, strengthen on the same order as a much coarser microstructure with more significant grain boundary precipitation. This demonstrates the role of the dislocations as heterogeneous matrix nucleation sites for both T_1 and θ' precipitates.

The trend of decreasing volume fraction for each precipitate with increasing pre-age stretch introduced some controversy. It is paramount to consider the error associated with the stereological correction method that was used for our analysis. The current method employed may have significant error associated with correcting an inhomogeneous microstructure comprised of truncated and very large plates. The measured diameter for any truncated plate was significantly increased by the correction program in order to normalize the average plate diameter, bringing truncated and finer plates closer to the mean length. This method enhances the corrected diameter and volume fraction values for the coarse microstructures of the non- and low-stretch specimens. The decreasing calculated volume fraction for T_1 and θ' may simply be accentuated by the correction method. As in the analysis for the isochronal treatment there is significant error associated with the calculated volume fraction of δ', which prohibits quantitative discussion.

There may also be thermodynamic suppressive forces that explain the dramatic volume fraction trend in the quantified microstructural analysis. The high number density of fine matrix plates may introduce significant capillary effects that essentially shift the phase boundaries for a given dislocation density, with greater the number density the more significant the effect [35]. Therefore, the greater the matrix precipitation of fine plates, the greater the pressure effects which shift the

phase boundaries essentially driving less of the equilibrium phases to precipitate.

Ultimately, this second investigation illustrated that material of a given strength may have vastly different microstructures. The quantitative results indicate that a large number of fine precipitates strengthen just as well as a fewer number of large precipitates with more significant grain precipitation. Future studies should focus on other related properties between materials with a given strength. Investigations into the fatigue properties, creep response and environmental resistance should be of particular interest for AF/C 458.

4.2. Theoretical modeling and simulation

Using the quantified data of T_1, θ' and δ' precipitate structures for each specimen, we conducted dislocation slip modeling (for details of the method, c.f. [16]) and evaluated the associated yield strength. In the simulation, we assumed that T_1 and θ' with {1 1 1} and {1 0 0} habit planes, respectively, to be unshearable during small plastic deformation until yielding. The δ' precipitate required an order-strengthening mechanism with strength

$$F = \pi/2 r_{\delta'} \gamma_{apb}, \tag{2}$$

where $r_{\delta'}$ is the radius of the δ' particle and the antiphase boundary energy $\gamma_{apb} = 0.07\ J/m^2$. Approximately 8000–15 000 obstacles formed by the intersection of the T_1, θ' and δ' with a {1 1 1} plane were taken into account in a square of certain area (according to the volume fraction of the particles) in the slip plane. An applied stress under which a dislocation line slips out of the area, that is, a micro-slip (plastic deformation) is generated, is assumed to correspond to the contribution σ_p of the precipitates to the total yield stress. Strengthening from grain boundaries and dispersoids (Al_3Zr and $Al_{20}Mn_3Cu_2$) are considered relatively small and constant throughout aging. Solid solution strengthening from Li and Cu in the matrix was considered; every 1 at.% Li gave rise to a 7 MPa increase [36] and 1 at.% Cu gave rise to 4 MPa [37], while the matrix contribution was 45 MPa [37].

Table 5 summarizes the results for the specimens aged at 150°C for 24 h after different stretches and Table 6 for the specimens aged to the yield strength of 450 MPa under various thermomechanical conditions. These tables illustrate that the computer simulation furnished an excellent method to evaluate and predict the yield strength associated with the various complex precipitate structures generated by the pre-age stretch and artificial aging treatments.

As previously described, the competitive precipitation between T_1, θ' and δ' and the associated mechanical properties are extremely sensitive to pre-age deformation as well as the artificial aging times. For a simple case of only two kinds (A and B) of plate-like precipitates (for instance θ' and T_1), as shown in [16] the computer simulations may offer an approach to find the optimum competitive precipitate structure for the associated strengthening stresses using a characteristic parameter κ_{AB} introduced as

$$\kappa_{AB} = \zeta\left(\frac{D_A}{D_B}\right)^2 \Bigg/ \left(\frac{\gamma_A}{\gamma_B}\frac{V_{m.A}}{V_{m.B}}\frac{\sin\theta_A}{\sin\theta_B}\right), \tag{3}$$

where the coefficient ζ accounts for the effect of the orientation of the plates ($\zeta = 3/4$ for θ'- and T_1-precipitates), D_A and γ_A are the mean diameter and the aspect ratio of the A-plates, respectively, and D_B and γ_B are those associated with the B-plates. The terms $V_{m.A}$ and $V_{m.B}$, θ_A and θ_B are the molar volumes and dihedral angles of the A and B plate-like particles with reference to the slip plane. For more complex structures consisting of three or more kinds of precipitates, as in AF/C 458, more structural parameters are necessary, which may be obtained through further experiments and computer simulations, to determine the optimum structure. Based on the simulations, the practical approach of implementing a pre-age stretch and aging treatment may be developed to acquire the optimum structures for the given mechanical properties of the alloy.

5. Conclusions

1. Pre-age plastic deformation enhances the aging kinetics, strength and number density of fine strengthening precipitates through the introduction of heterogeneous matrix nucleation sites.
2. The pre-age deformation significantly affects the competitive matrix precipitation between T_1 and θ'.
3. The relative volume fraction of T_1 to θ' is greatly increased with increasing amounts of deformation prior to artificial aging. The larger ΔG_v and the accomodation of the {1 1 1} shear strain for T_1 versus the {1 0 0} shear strain for θ' aids in its preferential nucleation on dislocations over that of θ'.
4. Specimens with a given strength may have vastly different microstructures without changing chemistry; only a single thermo-mechanical processing step is necessary.
5. Combining the dislocation-slip modeling with experimental tests, a practical approach to the optimization of mechanical properties for AF/C 458 may be developed.

Acknowledgements

The authors would like to acknowledge the helpful discussions with Professors Gary J. Shiflet and James M.

Howe and financial support of the Air Force Office of Scientific Research under Grant No. F49620-97-1-1034, Drs. Spenser Wu and Craig S. Hartley, Program Monitors.

References

[1] J.M. Silcock, J. Inst. Met. 88 (1959–60) 357–364.
[2] B. Noble, G.E. Thompson, Met. Sci. J. 6 (1972) 167–174.
[3] F.S. Lin, S.B. Chakrobortty, E.A. Starke Jr., Metall. Trans. A 13A (1982) 401–410.
[4] R.E. Crooks, E.A. Starke Jr., Metall. Trans. A 15A (1984) 1367–1377.
[5] R.F. Ashton, D.S. Thompson, E.A. Starke Jr., F.S. Lin, in: C. Baker, P. Gregson, S. Harris, C. Peel (Eds.), Aluminum–Lithium III, vol. III, The Institute of Metals, London, 1986, pp. 66–77.
[6] R.J. Rioja, P.E. Bretz, R.R. Sawtell, W.H. Hunt, E.A. Ludwiczak, in: Proceedings of the International Conference on Aluminum Alloys – Physical and Mechanical Properties, vol. III, Chameleon Press, London, 1986, pp. 1781–1797.
[7] J. White, W.S. Miller, I.G. Palmer, R. Davis, T.S. Sani, in: C. Baker, P. Gregson, S. Harris, C. Peel (Eds.), Aluminum–Lithium III, vol. III, The Institute of Metals, London, 1986, pp. 375–383.
[8] J. White, W.S. Miller, in: G. Champier, B. Dubost, D. Miannay, L. Sabety, (Eds.), Aluminum–Lithium IV, vol. IV, les editions de physique, Les Ulix Cedex, France, 1987, pp. 425–431.
[9] R.J. Sinko, T. Ahrens, G.J. Shiflet, E.A. Starke Jr., in: T.H. Sanders Jr., E.A. Starke Jr., (Eds.), Aluminum–Lithium Alloys V, vol. V, 1989, pp. 375–383.
[10] T. Ahrens, E.A. Starke Jr., in: T.H. Sanders Jr., E.A. Starke Jr., (Eds.), Aluminum–Lithium Alloys V, vol. V, 1989, pp. 385–396.
[11] W.A. Cassada, G.J. Shiflet, E.A. Starke Jr., Metall. Trans. A 22A (1991) 287–297.
[12] W.A. Cassada, G.J. Shiflet, E.A. Starke Jr., Metall. Trans. A 22A (1991) 299–306.
[13] J.D. Kim, J.K. Park, Metall. Trans. A 24A (1993) 2613.
[14] S.P. Ringer, B.C. Muddle, I.J. Polmear, Metall. Mater. Trans. A 26A (1995) 1659–1671.
[15] A.K. Hopkins, K.V. Jata, R.J. Rioja, Mater. Sci. Forum (1996) 421–426.
[16] A.W. Zhu, A.A. Csontos, E.A. Starke Jr., Acta. Mater. 47 (6) (1999) 1713–1721.
[17] Annual Book of ASTM Standards, Metals Test Methods and Analytical Procedures Section 3, ASTM, Philadelphia, PA, 1993.
[18] A.A. Csontos, E.A. Starke Jr., Metall. Mater. Trans. A 31A (2000) 1965–1976.
[19] P.M. Kelly, A. Jostens, R.G. Blake, J.G. Napier, Phys. Stat. Sol. A 31 (1975) 771–780.
[20] M. Otten, Philips Electron Optics – Applications Laboratory, Building AAE, The Netherlands.
[21] S.A. Saltykov, Stereometrische Metallographie, Deutcher Verlag fur Grundstoffindustrie, Leipzig, Federal Republic of Germany, 1974.
[22] E.E. Underwood, Quantitative Stereography, Addison-Wesley, Reading, MA, 1970.
[23] D.A. Porter, K.E. Easterling, Phase Transformations in Metals and Alloys, second ed., Chapman & Hall, London, 1993 (reprinted).
[24] E. Hornbogen, in: E.A. Starke Jr., T.H. Sanders Jr., W.A. Cassada (Eds.), Seventh International Conference on Aluminum Alloys: Their Physical and Mechanical Properties, Trans Tech Publications Ltd, Switzerland, 2000, pp. 879–888.
[25] J.W. Cahn, Acta Met. 5 (1957) 169–172.
[26] J.W. Martin, R.D. Doherty, B. Cantor, Stability of Microstructure in Metallic Systems, second ed., Cambridge University Press, Cambridge, MA, 1997, p. 58.
[27] J.C. Huang, A.J. Ardell, in: G. Champier, B. Dubost, D. Miannay, L. Sabety, (Eds.), Aluminum–Lithium IV, vol. IV, les editions de physique, Les Ulix Cedex, France, 1987, pp. 373–383.
[28] L. Löchte, A. Gitt, G. Gottstein, I. Hurtado, Acta Mater. 48 (2000) 2969–2984.
[29] E. Hornbogen, Aluminium 43 (1967) 41, 115, 163.
[30] D.Y. Li, L.Q. Chen, Acta Mater. 46 (1998) 2573–2585.
[31] S.F. Baumann, D.B. Williams, Scripta Metall. 18 (1984) 611–616.
[32] R.B. Nicholson, Phase Transformations, Chapman & Hall, London, 1970, p. 269.
[33] J.F. Nie, H.I. Aaronson, B.C. Muddle, in: M. Koiwa, K. Otsuka, T. Miyazaki (Eds.), The Japan Institute of Metals Proceedings, Volume 12 (JIMIC-3), Solid–Solid Phase Transformations, Part I, 1999, pp. 1128–1135.
[34] B.C. Muddle, J.F. Nie, in: M. Koiwa, K. Otsuka, T. Miyazaki (Eds.), The Japan Institute of Metals Proceedings, Volume 12 (JIMIC-3), Solid–Solid Phase Transformations, Part II, 1999, pp. 157–160.
[35] G.J. Shiflet, Department of Materials Science and Engineering, University of Virginia, Personal communication 4/26/2000.
[36] B. Noble, S.J. Harris, K. Dinsdale, Met. Sci. 16 (1982) 425.
[37] J.R. Davis, Aluminum and Aluminum Alloys – ASM Special Handbook, The Materials Information Society, Materials Park, OH, 1993, pp. 49.

Materials Science Forum Vols. 331-337 (2000) pp. 1333-1340

APPENDIX III

The Effect of Quench Rate on the Microstructure and Properties of AF/C-458 and AF/C-489 Al-Li-Cu-X Alloys

A.A. Csontos[1], B.M. Gable[1], A. Gaber[2] and E.A. Starke, Jr.[1]

[1] Department of Materials Science and Engineering, University of Virginia, Charlottesville, VA 22901, USA

[2] Physics Department, Assiut University, Assiut, 71516, Egypt

Keywords: Aerospace Materials, Aluminium-Lithium Alloys, Pre-Age Stretch, Quench Sensitivity

ABSTRACT

The Air Force recently developed two isotropic Al-Li-Cu-X alloys with 1.8^{w}/$_{o}$Li and 2.1^{w}/$_{o}$Li designated AF/C-458 and AF C-489, respectively. The objective of this investigation was to determine the effect of quench rate on the microstructure and mechanical properties of the AF/C-458 and AF/C-489 alloys. TEM, SEM, microhardness, and tensile testing were utilized to ascertain these microstructure/property relationships for both alloys in the T4, T6, and T86 tempers as a function of quench rate. Subsequent losses in ductility for both alloys in all tempers with decreasing quench rate were determined to be due to the precipitation of the equilibrium Al_2CuLi (T_1) phase along subgrain and grain boundaries which promoted intergranular fracture. Furthermore, yield and tensile strengths increased for both alloys in the T4 temper but decreased in the T6 and T86 tempers with decreasing quench rate. The increased strengths for the T4 condition resulted from the heterogeneous precipitation of coarse T_1 and naturally aged δ' phases. The decrease in yield and tensile strengths for the T6 and T86 tempers were also due to the coarse heterogeneous precipitation of T_1 which denuded regions of Cu thereby reducing the number density of fine matrix θ" (T6) and T_1 (T86). Finally, a comparison of the quench sensitivity for both the AF/C-458 and AF/C-489 alloys indicates that the mechanical properties for both alloys were less quench rate sensitive than other typical Al-Li-Cu-X alloys.

I. INTRODUCTION & BACKGROUND

In this era of streamlined economics for the aerospace industry, weight reduction of aerospace vehicles is best achieved through reducing the density of the aircraft's structural materials. For aluminum alloys, lithium is added to reduce the alloy's density with the added benefit of increasing the strength and elastic modulus of the alloy. Most Al-Li-X alloys have achieved approximately 10% reduction in density and approximately 10% increase in elastic modulus [1-4]. The major strengthening component of binary Al-Li alloys arises from the precipitation of the metastable spherical Al_3Li (δ') phase. The δ' possesses a Ll_2 ordered structure, which nucleates more or less homogeneously in Al-Li-Cu-X alloys upon quenching or natural aging with lithium contents greater than 5.8^{a}/$_{o}$Li (1.6^{w}/$_{o}$Li). Due to their ordered structure and high degree of coherency with the matrix, δ' precipitates can lead to undesirable planar slip [5] by the concomitant shearing of these δ' with each passing dislocation which effectively softens the active slip plane, thus, resulting in coarse planar slip. The addition of Cu and Mg to Al-Li alloys lowers the solubility of lithium which drives the δ' precipitation and may lead to precipitation of other strengthening phases that may homogenize deformation, namely Al_2Cu (θ' & θ"), Al_2CuMg (S') and Al_2CuLi (T_1). In addition, phases such as AlLi (δ), Al_6CuLi_3 (T_2) and Al_7Cu_4Li (T_B) may precipitate through artificial aging or slow cooling from the solution heat treatment in supersaturated alloys at intermediate temperatures [6,7].

Quench sensitivity is a measure of the precipitation of these metastable and equilibrium phases during an imposed quench from the solutionizing anneal. In Al-Li-Cu-X alloys, the

dissolved elements have a decreasing solubility with decreasing temperature, thus, when the alloy is cooled from the solutionizing anneal, the quench rate determines whether a supersaturated solid solution forms or rather solute rich precipitates form. If the quenching rate is sufficiently rapid there is insufficient time for atomic migration to form precipitates, thus, forming a supersaturated solid solution. However, at slow quenching rates, there may be sufficient time for solute atomic migration, which promotes precipitation at high-energy locations, e.g. grain boundaries, of the equilibrium phases. The type, size, and location of these precipitates strongly affect the subsequent microstructural evolution, fracture behavior, and mechanical properties of these alloys.

Typically, the more solute present in the alloy, the higher the quench sensitivity of the alloy. Alloys which fail to achieve their optimum properties due to the implementation of slower quench techniques are considered to be quench sensitive. Limited information regarding the effect of quench sensitivity on the microstructure and mechanical properties of Al-Li-Cu-X alloys has been established [8-15]. A quantitative study has been performed elsewhere [8] which relates the quenching rate to the microstructure and toughness of both lean and rich AA8090 alloys. The obtained results of this study conveyed a good correspondence between the loss of fracture resistance with the increase in volume fraction of T_2 and Al_2CuMg (S) phases. The most rapid loss in fracture resistance for both alloys occurred as a result of isothermal aging at relatively high temperatures (400 - 450°C) where T_2 precipitates were dominant. These results were supported by another study [9] that showed that the influence of quenching rate on the mechanical properties of AA8090, AA2091, and two CP276 alloys were temper dependent.

II. Experimental Procedure

The unrecrystallized ¼" thick AF/C-458 (Al-2.7Cu-1.8Li-0.6Zn-0.3Mg-0.3Mn-0.08Zr (wt%)) and ½" thick AF/C-489 (Al-2.7Cu-2.1Li-0.6Zn-0.3Mg-0.3Mn-0.05Zr (wt%)) plates used in this study were fabricated by Alcoa and the Air Force Research Labs, respectively. Both alloys were direct chill cast, stress relieved, homogenized, hot rolled, annealed at 540°C for 4 hrs, and then slow cooled before hot rolling again. This was followed by a solution anneal at 540°C for 1 hour and an immediate water quench. A 6% pre-age stretch was provided, therefore, the T36 temper for both AF/C-458 and AF/C-489 alloys served as the "as-received" material from which all solutionizing and quenching operations occurred.

Tensile specimens were machined in accordance with ASTM E8-93 from the received plates so that the gauge lengths were parallel to the rolling direction. The tensile tests and pre-age stretching were performed on a MTS 10/GL Sintech test frame at a constant crosshead displacement of 3mm/min. Vickers microhardness specimens were machined from their respective received plate with dimensions of 4x5x10 mm. The Vickers microhardness measurements were performed using the Vickers indenter on polished surfaces under a load of 4.9 Newtons for a duration of 10 seconds. Each hardness value was obtained from the average of at least ten random measurements. Both tensile and Vickers microhardness specimens were solution heat treated in a Lindberg three-zone furnace at 550°C for 30 minutes and subsequently quenched in water, glycerol, or still air and immediately stretched and/or aged. For the T86 temper, the 6% pre-age stretch was performed immediately upon quenching from the solution heat treatment to minimize the effects of an inhomogeneous planar dislocation structure due to the natural aging of the fine shearable δ' precipitates. The tensile and Vickers microhardness samples were then aged in a Stabil-Therm forced air box furnace at 150°C for 32 hours and 24 hours for the T6 and T86 tempers, respectively. To quantitatively measure the quench rate of both the tensile and Vickers microhardness samples, a hole approximately 1.5mm in diameter was drilled on one side of dummy specimens to a depth of approximately 2mm. A K-type thermocouple was inserted tightly in the hole to monitor the temperature change with time during the quench. The resulting data yielded quenching rates for the tensile samples to be 290°C/sec in water, 68°C/sec in glycerol, and 1.8°C/sec in still air while the

smaller Vickers specimens were determined to be 500°C/sec in water, 130°C/sec in glycerol, and 3°C/sec in still air. Digital SEM fractographs were acquired through the use of a DSM982 Gemini field-emission SEM operating at 10kV equipped with dual backscatter electron detectors, one perpendicular and the other at 45° to the surface. A JEOL 2000FX conventional microscope was utilized for TEM after samples were mechanically thinned, punched into 3mm disks, and electropolished in a Tenupol twin-jet electropolisher with a 3.5:1 methanol: nitric acid solution.

III. Results & Discussion

As-Received T36 Condition

Prior research [16] quantitatively demonstrated that the smaller grained AF/C-458 alloy possess an aspect ratio roughly twice that of the larger grained AF/C-489 plate where the number of grains were 2.5 to 3 times greater in the AF/C-458 alloy than in the AF/C-489 plate. Furthermore, the unrecrystallized grain structure of both alloys was confirmed by low magnification TEM which demonstrated an approximate 5-10μm sub-grain size.

As-Quenched and Naturally Aged T4 Condition

Due to δ' precipitation during the quench and resulting natural aging, analysis of the T4 temper is separated into the as-quenched T4 and naturally aged T4 conditions, which represents those microstructures and mechanical properties acquired within the first 2 hours after quenching and after 48 hours at room temperature, respectively. Previous investigations [16] indicate that δ' natural aging occurred rapidly after quenching and nearly reached peak hardness after just 8 hours at room temperature. The as-quenched microhardness values for both AF/C-458 and AF/C-489 are illustrated in Figure 1. The higher Li content AF/C-489 alloy exhibits greater hardness values over the leaner AF/C-458 at the slower quench rates, with only a slight increase in hardness for the water quench. As seen in Figures 2a&b, the difference in the hardness with decreasing cooling rate from the solution heat treatment may be directly attributed to δ' and T_1 precipitation during the quench.

The as-quenched T4 and naturally aged T4 tensile data for the water, glycerol and air quenched specimens are illustrated in Table 1. The water and glycerol quenched samples, for both AF/C-458 and AF/C-489, exhibited similar properties, however, the air cooled specimens displayed strengths 30-40% higher and elongations 62% and 82% lower, respectively. As seen in Figures 2a&b, the significantly increased strengths and reduced ductility for the air cooled T4 AF/C-458 and AF/C-489 alloys is associated with coarse T_1 precipitation during the quench. Furthermore, the slightly higher strengths in the water quenched over the glycerol quenched specimens was most likely due to the initial stages of δ' natural aging where the increased number of quenched-in vacancies from the rapid water quench enhanced Li diffusivity thereby δ' precipitation and the strengthening effect. Also, note the mechanical property differences between the two alloys where the AF/C-458 exhibits higher strengths and elongations than the AF/C-489 alloy for similar conditions. As previously reported [16], the differences in strength and ductility arise from the much finer grain structure of the AF/C-458 alloy in comparison to the AF/C-489 plate, which acts to reduce the slip length, subsequent strain localization, and premature intergranular fracture. In other words, the increased strengths

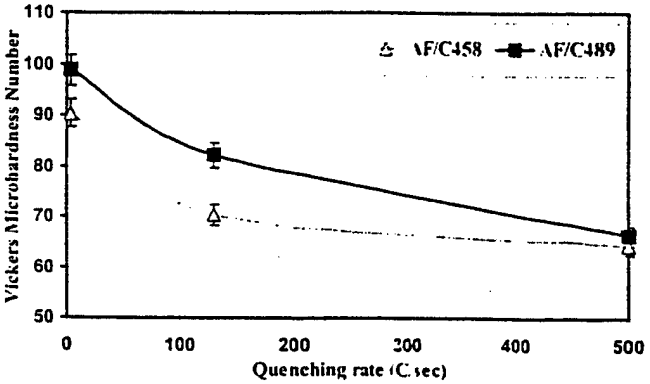

Figure 1. As-quenched Vickers Microhardness vs. Quenching Rate

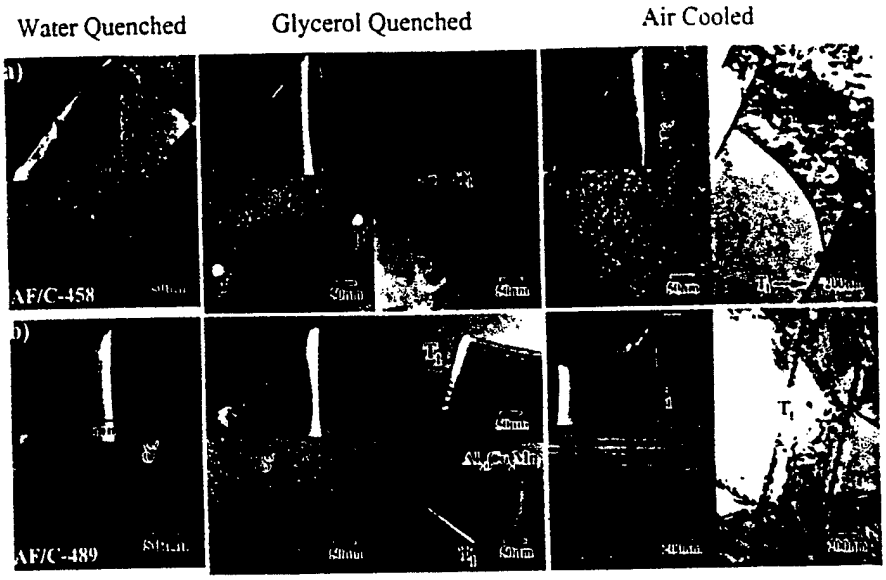

Figure 2. a-b) As-quenched T4 SEM fractographs & TEM micrographs B=[011], g=⅓[200]δ', g=½[111]T_1.

and elongations for the finer-grained AF/C 458 alloys with qualitatively similar low precipitate volume fractions may be attributed to Hall-Petch strengthening and reduced strain localization, respectively.

As shown in Table 1 for the AF/C-458 alloy, the water and glycerol quenched specimens exhibit higher strengths and lower ductility due to the natural aging of the δ' precipitates, i.e. T4 2 H vs. T4 48 H. Vickers microhardness data also demonstrates this trend for the water and glycerol quenched samples, however, no natural aging trend was found for the air cooled condition. As seen in Figure 2a-air cooled, the lack of natural aging can be attributed to the air cooled microstructure where fine δ' particles have already precipitated to a large extent during the quench. Finally, both the AF/C-458 and AF/C-489 alloys were determined to be less quench sensitive when compared to both T4 AA8090 and AA2090 mechanical properties as a function of quench rate.

Quench Media	Aging Temper	AF/C-458 Alloy			AF/C-489 Alloy		
		YS (MPa)	UTS (MPa)	Elongation (%)	YS (MPa)	UTS (MPa)	Elongation (%)
Water Quench (290°C/sec)	T4 2H	161	287	25.3	142	268	23.2
	T4 48H	205	352	19.4	-	-	-
	T6	323	446	12.5	288	427	11.6
	T86	501	537	10.3	500	554	4.8
Glycerol Quench (68°C/sec)	T4 2H	150	275	26.1	129	255	23.3
	T4 48H	146	303	21.3	-	-	-
	T6	296	416	13.2	231	363	8.5
	T86	360	413	6.6	334	392	3.9
Air Cooled (1.8°C/sec)	T4 2H	225	369	15.6	189	337	12.8
	T6	299	421	9.8	214	362	8.2
	T86	411	455	6.9	412	433	3.0

Table 1. Tensile Data for the Various Quenching Conditions

T6 Condition (150°C for 32 hrs)

After the solutionizing anneal and respective quenches, the tensile samples were then peak aged at 150°C for 32 hours and tested to obtain the mechanical property data in Table 1. The artificial age greatly increased the strength and reduced the ductility for both alloys in each quenching condition respective to the T4 temper. For both alloys, the water quenched specimens exhibited the best combination of high strengths and ductility while the air cooled samples showed the least ductility with strengths comparable to the glycerol quenched conditions. As seen in Figures 3a&b, these trends can be directly related to the fracture behavior and microstructure of both alloys as a function of quench rate.

The SEM fractographs clearly show the grain size variation between the alloys and that both water quenched and AF/C-458 glycerol and air cooled samples fractured at 45° and contained mostly transgranular shear, whereas the glycerol and air cooled AF/C-489 contained mostly intergranular fracture. Furthermore, the TEM investigation of both alloys generally found larger and higher volume fraction δ' and sub-grain and grain boundary T_1 precipitates coupled with a fine and highly dense matrix dispersion of θ" with respect to the T4 temper. In particular, the water quenched specimens for both alloys exhibited similarly sized T_1 plates along sub-grain and grain boundaries as well as residual matrix dislocations and incoherent dispersoid/matrix interfaces while the glycerol and air cooled samples showed a bimodal distribution of similarly located T_1. This T_1 bimodal distribution suggests that the larger T_1 plates nucleated during the slower quench and grew with the artificial age while the smaller T_1 nucleated and grew only during the age. These large T_1 plates also effect the competing θ" precipitation as seen by the glycerol quenched AF/C-489 TEM micrograph. The large grain boundary penetrating T_1 plate denuded the adjacent area of Cu, which prevented the fine θ" precipitation and produced a precipitate free zone (PFZ) surrounding the T_1 plate. As seen by the slower quenched mechanical property data, these PFZs reduce the strength and ductility of these alloys by preventing matrix precipitation of the major strengthening θ" phase for this T6 temper and by promoting strain localization, respectively.

Also note that the AF/C-458 strength and ductility levels were 5-40% and 8-55% greater, respectively, when compared to similar AF/C-489 samples with the least difference from the water quenched condition. This disparity between the alloys indicates that along with the differences in Li content and, thus, δ' volume fraction, grain size may also have a large effect on the mechanical properties which may not be due to the quenching conditions specifically. Initial observations, as seen in Figures 3a&b, clearly suggest that the differences between the alloys may be due in part to the grain size variation and correspondingly to the increased propensity for intergranular fracture with decreasing quenching rate, e.g. AF/C-489. As mentioned previously, earlier work [16] quantitatively showed that the grain size and δ' volume fraction was ~3 times larger and ~3% greater, respectively, in the 2.1 wt%Li AF/C-489 alloy when compared to the 1.8 wt%Li AF/C-458 alloy in the T36 and T86 (150°C 24 hour) tempers. We may assume for the T6 condition that the ~3% δ' volume fraction difference between the two alloys should not change dramatically since the 6% pre-age stretch should only affect the amount of the spherical and coherent δ'(Al_3Li) indirectly through the preferred precipitation of T_1(Al_2CuLi) at the expense of θ" (Al_2Cu). Thus, the lower strength and ductility levels of the T6 AF C-489 alloy may be attributed to the significantly larger grain size and increased volume fraction of shearable δ' which both substantially increase the amount of strain localization at grain boundaries, resulting in more low energy intergranular fracture.

T86 condition (150°C for 24hrs)

A pre-age 6% stretch was incorporated for both alloys following the solution anneal and corresponding quenches to increase the competitive precipitation of T_1 during the 150°C 24 hour age. The 6% pre-age stretch was utilized because T_1 nucleation has been shown to be greatly

Figure 3. a&b) T6 (150°C 32H) AF/C-458 & AF/C-489 SEM fractographs & TEM micrographs showing transgranular/intergranular fracture and δ', θ", & T_1 precipitation, B=[110], g=½[200]δ',θ", g=½[111]T_1.

influenced by dislocation jogs [17,18] while prior research [19] determined that the 6% stretch optimized the tensile properties with the least amount of stretch. The tensile data, as seen in Table 1, shows that the pre-age stretch resulted in marked strength increases and lower elongations as compared to similarly quenched T4 and T6 samples. As in the T6 condition, the water quenched specimens exhibited the highest strengths and ductility while the air cooled samples showed the least ductility with strengths actually 10-20% higher than the glycerol quenched conditions. Unlike the T6 condition, the yield and tensile strengths were remarkably similar between the respective AF/C-458 and AF/C-489 quenched samples, however, the ductility of the AF/C-489 samples were

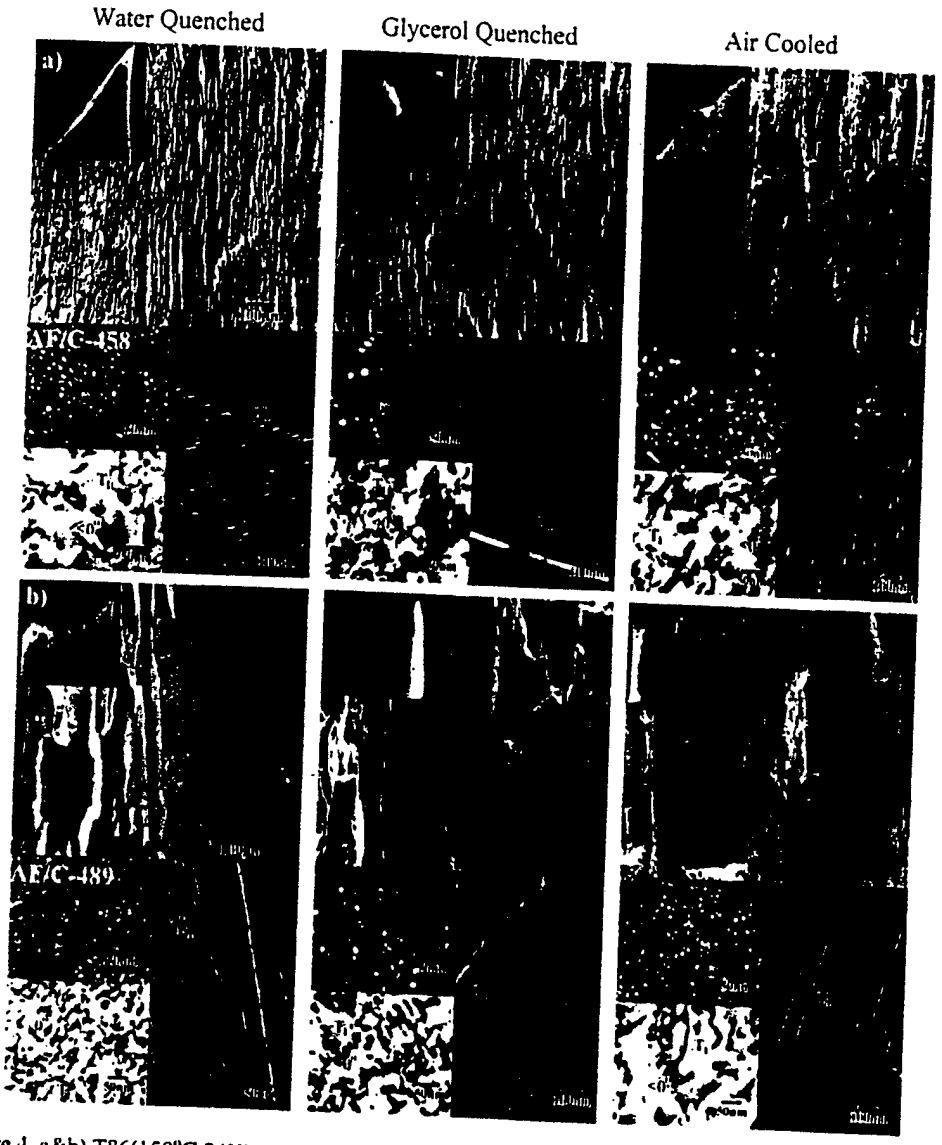

Figure 4. a&b) T86(150°C 24H) AF C-458 & AF/C-489 SEM fractographs & TEM micrographs showing transgranular/intergranular fracture and δ', θ", & T_1 precipitation, B=[110], g=½[200]δ',θ", g=½[111]T_1.

41-57% lower than the AF/C-458 alloy. These trends are also related to the fracture behavior and microstructure of both alloys as a function of quench rate.

As seen in Figure 4a&b, the SEM fractographs again illustrate the differences in grain size and fracture mode for both alloys, i.e. mostly transgranular shear for the AF/C-458 water quench and varying amounts of intergranular fracture with the worst being the air cooled AF/C-489 alloy. Although not presented here for brevity, high magnification SEM fractography indicated that intergranular fracture did play a role in the low ductility of the AF/C-458 glycerol and air cooled conditions. The significantly higher strengths for the T86 temper can be directly related to the increase in matrix T_1 volume fraction and number density at the expense of the θ" precipitate. Also,

note again the bimodal distribution of the T_1 plates that formed during the slower quenches for both AF/C-458 and AF/C-489 samples. Furthermore, the only noticeable difference to account for the 10-20% lower strengths of the glycerol quenched as compared to the air cooled samples was the apparent lower δ' volume fractions for the glycerol quenched specimens, although more work on this point needs to be addressed. Once again, the low ductility of the AF/C-489 alloy in comparison to the AF/C-458 alloy of similar quenching conditions was attributed to the ~3% higher volume fraction of δ' coupled with the larger grain size. Thus, both factors significantly increase the amount of strain localization and stress concentrations at grain boundaries, which resulted in more low energy intergranular fracture for the AF/C-489 alloy.

IV. Conclusions

This research has shown the effect of quench rate on the microstructural evolution and overall mechanical behavior of the T4, T6, and T86 AF/C-458 and AF/C-489 alloys. A more rapid quench was determined to be more desirable for optimizing the strengths and ductility for both alloys. The AF/C-489 alloy appears to be more quench sensitive than AF/C-458 due to the higher solute content and larger grain size. Nevertheless, both AF/C-458 and AF/C-489 alloys were shown to maintain lower quench sensitivity values than their T4 Al-Li-Cu-X counterparts AA8090 & AA2090.

Acknowledgements

This research was funded under Air Force Office of Scientific Research Grant F49620-97-1-1034.

VI. References

[1] D.B. Williams, R. Levi-setti, J.M. Chabala, Y.L. Wang, D.E., Newbury, Appl. Surface Sci. 37, 78 (1989).
[2] A. Yamamato, H. Tsubakino, R. Nozato, 4th Inter. Conf. On Al alloys, ed. by E.A. Starke, Jr, T.H. Sanders, Jr, Vol. II, Atlanta, Georgia, USA (1994) P. 191.
[3] A.F. Smith, J. de Physique, 48C_3-49 & C_3-629 (1987).
[4] A.F. Smith, Mater. Sci. Technology, 5, 533 (1989).
[6] E.A. Ludwiczak and R.J. Rioja, Scripta Metall. Mat., 25, 1415 (1991).
[7] K.S. Prasad, A.K. Mukhopadhyay, A.A. Gokhale, D. Benerjee and D.B. Goel, Scripta Metall. Mat., 30, 1299 (1994).
[8] G.N. Colvin, E.A. Starke.Jr, SAMPE Quarterly, 19, 10 (1988).
[9] G.Lapasset, C.Damerval, M.Doudeau, 5th Inter. Conf. on Al-Li alloys, Williamsburg, VA, March 27-31, 365 (1989).
[10] S.Hirano, H.Yoshida, T.Uno, *ibid.* 335 (1989).
[11] J.T. Staley, R.D. Doherty, *ibid.* 345 (1989).
[12] M.E. Donnellan, W.E. Frazier, *ibid.* 355 (1989).
[13] J.T. Staley, Mater. Sci. Technol., 3, 923 (1987).
[14] J.T. Staley, PhD Thesis, " Modeling quenching of precipitation strengthened alloys – Application to an Al-Cu-Li Alloy", Drexel University (USA), 1989.
[15] P.A. Rometsch, G.B. Schaffer, Ji-Yong Yao, M.J. Couper, Proceed. 6th Int. Conf. on Al-Alloys, Toyhashi-Japan, July 5-10,1998. Ed. T. Sato, S. Kumai, T. Kobayashi, Y. Murakami.
[16] A.A. Csontos, E.A. Starke, Jr., Met. Trans, In Press (2000)
[17] W.A. Cassada, G.J. Shiflet, and E.A. Starke, Jr., Metall. Trans. A., Vol. 22A, 1991, p. 287.
[18] W.A. Cassada, G.J. Shiflet, and E.A. Starke, Jr., Metall. Trans. A., Vol. 22A, 1991, p. 299.
[19] B. Gable, A.A. Csontos, and E.A. Starke, Jr., paper in progress

DISTRIBUTION LIST

1 - 3	Dr. Craig S. Hartley Program Manager, Metallic Materials Directorate of Aerospace and Mechanical Sciences Air Force Office of Scientific Research 801 N. Randolph St. Arlington, VA 22203-1977
4	SEAS Postaward Administration
5 - 6	E. A. Starke, Jr.
7	W. A. Jesser
8 - 9	M. Rodeffer, Engineering Library, Clark Hall
10	SEAS Preaward Administration Files

JO#0840:ph